Numerical solution of Riemann–Hilbert problems: random matrix theory and orthogonal polynomials

Sheehan Olver and Thomas Trogdon

February 22, 2013

Abstract

Recently, a general approach for solving Riemann–Hilbert problems numerically has been developed. We review this numerical framework, and apply it to the calculation of orthogonal polynomials on the real line. Combining this numerical algorithm with the approach of Bornemann to compute Fredholm determinants, we are able to calculate spectral densities and gap statistics for general finite-dimensional unitary invariant ensembles. We show that the accuracy of the numerical algorithm for approximating orthogonal polynomials is uniform as the degree grows, extending the existing theory to handle g-functions. As another example, we compute the Hastings–McLeod solution of the homogeneous Painlevé II equation.

1 Introduction

We are concerned with computing finite dimensional random matrix statistics for unitary invariant ensembles. These statistics are expressed in terms of orthogonal polynomials, Airy functions and Painlevé functions. The common thread is the presence of a Riemann–Hilbert (RH) representation. We take a computational approach to these RH representations which results in accurate numerical methods for calculating unitary invariant ensemble statistics. To the reader familiar with RH problems, our techniques pull from the method of nonlinear steepest descent including contour deformations and the so-called g-function technique. We adapt these techniques for numerical use, and analyse the resulting numerical algorithm, which requires extending the analysis of the numerical algorithm to the as-of-yet unconsidered case of g-functions.

Our primary focus are eigenvalue statistics of *unitary invariant ensembles*. Unitary invariant ensembles are $n \times n$ random Hermitian matrices

$$M = \begin{pmatrix} M_{11} & M_{12}^{\mathrm{R}} + \mathrm{i}M_{12}^{\mathrm{I}} & \cdots & M_{1n}^{\mathrm{R}} + \mathrm{i}M_{1n}^{\mathrm{I}} \\ M_{12}^{\mathrm{R}} - \mathrm{i}M_{12}^{\mathrm{I}} & M_{22} & \cdots & M_{2n}^{\mathrm{R}} + \mathrm{i}M_{2n}^{\mathrm{I}} \\ \vdots & \ddots & \ddots & \vdots \\ M_{1n}^{\mathrm{R}} - \mathrm{i}M_{1n}^{\mathrm{I}} & \cdots & M_{(n-1)n}^{\mathrm{R}} - \mathrm{i}M_{(n-1)n}^{\mathrm{I}} & M_{nn} \end{pmatrix}$$

whose entries are distributed according to

$$\frac{1}{Z_n} \mathrm{e}^{-n \operatorname{Tr} V(M)} \, \mathrm{d}M,$$

where Z_n is the normalization constant and

$$\mathrm{d}M = \prod_{i=1}^{n} \mathrm{d}M_{ii} \prod_{i<j} (\, \mathrm{d}M_{ij}^{\mathrm{R}} \, \mathrm{d}M_{ij}^{\mathrm{I}}),$$

for real-valued random variables M_{ij}^{I} and M_{ij}^{R}.

Eigenvalue statistics of invariant ensembles are expressible in terms of the kernel[1]

$$\mathcal{K}_n(x,y) = \gamma_{n-1}\mathrm{e}^{-n/2(V(x)+V(y))}\frac{\pi_n(x)\pi_{n-1}(y)-\pi_{n-1}(x)\pi_n(y)}{x-y},$$

where π_k are the monic polynomials $\pi_0, \pi_1, \ldots$ orthogonal to the weight

$$\mathrm{e}^{-nV(x)}\,\mathrm{d}x,$$

where

$$\gamma_{n-1} = \left[\int \pi_{n-1}^2(x)\mathrm{e}^{-nV(x)}\,\mathrm{d}x\right]^{-1}$$

is a normalization constant. Particular statistics include the *spectral density*

$$\mathrm{d}\mu_n = \frac{\mathcal{K}_n(x,x)}{n}\,\mathrm{d}x,$$

describing the global distribution of eigenvalues[2]. The *limiting spectral density* — the weak$\star$ limit of $\mathrm{d}\mu_n$ as $n\to\infty$ — is the *equilibrium measure* associated to the potential V [8, Section 6.4]. We also calculate *gap statistics*, describing the local distribution of eigenvalues; namely, the probability that no eigenvalue belongs to a set Ω. These are given by the Fredholm determinant [14, (4.65)]

$$\det(I-\mathcal{K}_n|_{L^2(\Omega)}),$$

where $\mathcal{K}_n|_{L^2[\Omega]}$ denotes the integral operator with kernel $\mathcal{K}_n$ on $L^2(\Omega)$.

Gap statistics for invariant ensembles follow two principles of universality. For x in the *bulk* — i.e., inside the support of the equilibrium measure — the gap statistic of a properly scaled neighbourhood of x approaches the sine kernel distribution[3]:

$$\rho^{\sin}(s) = \det(I-\mathcal{S}|_{L^2(-s,s)}) \quad \text{for} \quad \mathcal{S} = \frac{\sin(x-y)}{x-y}.$$

Moreover, the *edge statistic* — i.e., the probability that no eigenvalue lies in a properly scaled neighbourhood of ∞[4] — generically approaches the Tracy–Widom distribution:

$$\rho^{\mathrm{Ai}}(s) = \det(I-\mathcal{A}|_{L^2(s,\infty)}) \quad \text{for} \quad \mathcal{A} = \frac{\mathrm{Ai}(x)\mathrm{Ai}'(y)-\mathrm{Ai}'(x)\mathrm{Ai}(y)}{x-y}.$$

The literature proving the validity of these universality laws is extensive, see [2] for an overview. Of particular interest to the present paper are proofs for unitary invariant ensembles based on asymptotic analysis of RH Problems associated with orthogonal polynomials: for bulk statistics see [8] and for edge statistics see [9]. Underlying these two universality laws are *Painlevé transcendents*; in the case of the Tracy–Widom distribution it is the

[1] This form for the *unscaled* kernel comes form [6, (1.2)], though using the notation from the *scaled* kernel in [8, Chapter 8]. We have altered the definition of γ_{n-1} to avoid cancelling imaginary constants.

[2] This is also called the *one-point correlation function* [8, Section 6.4] or the *level density* [15, Figure 12.1]. We use spectral density in accordance with [2, Figure 1.1].

[3] Instead of scaling Ω, one can also scale the matrix itself in the statement of the universality law; cf. [3, Theorem 3.1.1]. Alternatively, one can rescale the kernel of the operator through a change of variables [8, Chapter 8]. We choose the convention of scaling only Ω and leaving the kernel unchanged.

[4] Another statement of the Tracy–Widom universality law is in terms of scaling the largest eigenvalue, cf. [3, Theorem 3.1.4]. We use a scaled neighbourhood of infinity in accordance with [6, (1.15)].

Hastings–McLeod solution to Painlevé II [20], whereas the sine kernel distribution is expressible in terms of a solution to Painlevé V [21]. These Painlevé representations can also be expressed as RH problems [16], which can be viewed as RH problems for the logarithmic derivative of $\rho^{\sin}$ and ρ^{Ai}, in contrast to the RH problems for the kernel $\mathcal{K}_n$ that we will calculate. See Appendix A for a discussion of a numerical RH approach for computing the Hastings–McLeod solution of Painlevé II.

The statistics differ from universality laws for finite n and, in general, there are no known expressions in terms of Painlevé transcendents. Hence our aim is to calculate the finite-dimensional statistics to explore the manner in which the statistics approach universality laws depends on the potential V. To accomplish this task, we calculate the associated orthogonal polynomials numerically, also using their Riemann–Hilbert representation, via the framework of [26, 27]. By deforming the contours appropriately, we realize a numerical method that is uniformly accurate for large and small n, as in [28].

An overview of the paper follows:

Section 2 We present the numerically calculated finite-dimensional invariant ensemble statistics. We see in our numerical experiments that the rate in which bulk statistics approach the universality law depends strongly on the magnitude of the density of the equilibrium measure (see Figure 4): where eigenvalue density is small, finite n statistics differ from universality behaviour greatly. Importantly, because we do not require the knowledge of local parametrices for the RH problem, our numerical approach continues to work for degenerate potentials, such as those that arise in the study of higher order Tracy–Widom distributions [6].

Section 3 We review the numerical method for Riemann–Hilbert problems of [27]. This includes conditions from [28] for the numerical approximation to be *uniformly accurate* with respect to a parameter (in our case n), when the contours are appropriately deformed and scaled (Section 3.2). This approach avoids the use of local parametrices, which are needed for the asymptotic analysis of RH problems.

Section 4 We alter the deformations of [8] for calculating orthogonal polynomials, to be incorporated into the numerical approach of Section 3. This includes (Section 4.1) a review of the numerical approach for calculating equilibrium measures and g-functions of [24].

Section 5 We adapt the resulting deformation to achieve uniform approximation, extending the theory of [28] for RH problems that use g-functions.

Remark As an alternative to manually deforming RH problems, an optimization algorithm can be used to automate the deformation process [34]. Unfortunately, support for g-functions is not yet incorporated, inhibiting the usefulness to the RH problems considered in this paper.

Remark An alternative to the approach advocated in this paper is to calculate the orthogonal polynomials directly for each n via modified Gram–Schmidt and numerical quadrature. For small n, this is likely to be more efficient. However, the number of quadrature points must greatly exceed n to ensure stability [19, Example 2.35]. Moreover, the calculation must be restarted for each n as the weight e^{-nV} changes. On the other hand, the RH approach has computational cost independent of n, making it more practical for investigating large n behaviour.

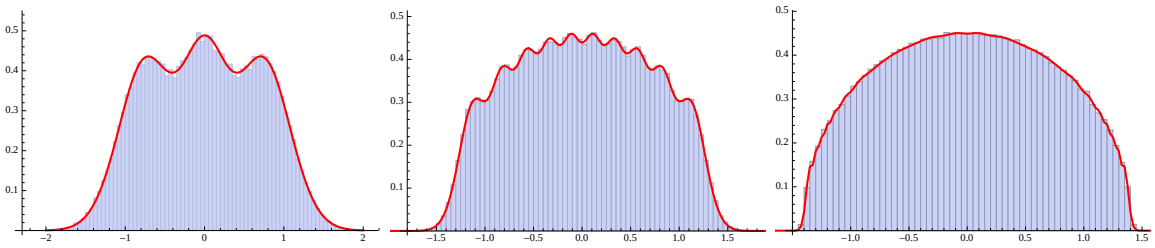

Figure 1: Calculated spectral densities for the GUE for $n = 3, 10$ and 100, compared to Monte Carlo simulation.

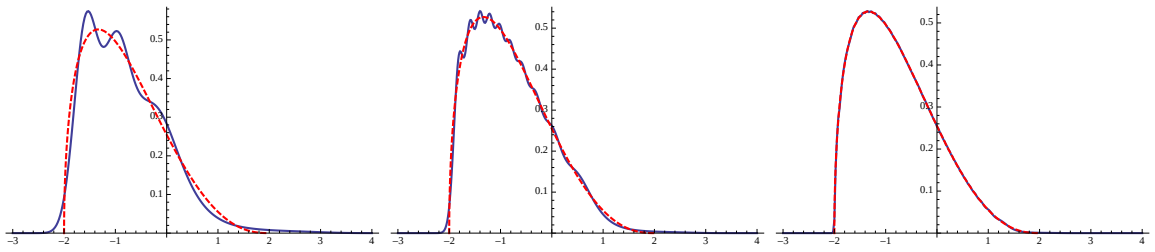

Figure 2: Calculated spectral density for $V(x) = \frac{x^2}{5} - \frac{4}{15}x^3 + \frac{x^4}{20} + \frac{8}{5}x$ for $n = 3, 10$ and 100. Dashed line is the equilibrium measure ($n = \infty$).

2 Finite-dimensional invariant ensemble statistics

In this section, we compute the finite n statistics of unitary invariant ensembles by using the numerical method for calculating π_n and $\gamma_{n-1}\pi_{n-1}$ that we develop in future sections. What is apparent in the numerical results is that the behaviour of local statistics is tied strongly to the global density of eigenvalues; i.e., the magnitude of the density of the equilibrium measure.

For unitary invariant ensembles, the spectral density is the distribution of the counting measure. In Figure 1, we compare the GUE (i.e., $V(x) = x^2$) spectral density (numerically calculated using our approach) for $n = 3, 10$ and 100 to a histogram, demonstrating the accuracy of the approximation. (Because the polynomials involved are Hermite polynomials, we also verify the accuracy directly.) This shows a phenomena where the distribution exhibits n "bumps" of increased density, likely corresponding to the positions of the finite charge energy minimization equilibrium; i.e., the Fekete points (see [32, Chapter III] for definition).

In Figure 2, we plot the finite n spectral densities for the potential

$$V(x) = \frac{x^2}{5} - \frac{4}{15}x^3 + \frac{x^4}{20} + \frac{8}{5}x,$$

which is an example of a potential whose equilibrium measure vanishes at an endpoint, and hence the edge statistics follow a higher order Tracy–Widom distribution [6]. Interestingly, this change in edge statistic behaviour is not just present in the local statistics, but clearly visible in the decay of the tail of the global statistics.

We turn our attention to local gap statistics, which are described by the *Fredholm determinant*

$$\det(I - \mathcal{K}_n|_{L^2[\Omega]}).$$

Using the method of Bornemann [5], we calculate the determinant, provided that the kernel itself can be evaluated. Thus, we successfully compute finite gap statistics by calculating

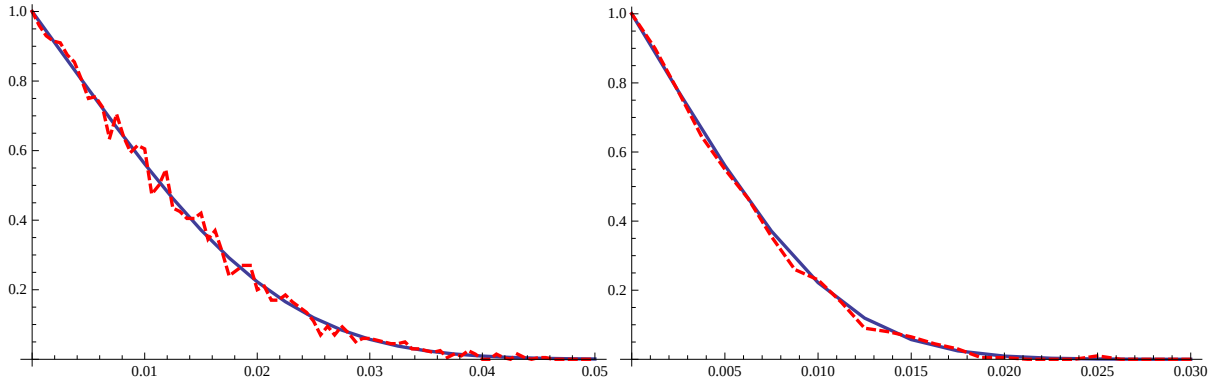

Figure 3: The calculated probability that there are no eigenvalues in $(-s, s)$ for the GUE (plain) versus Monte Carlo simulation (dashed), for $n = 50$ (left) and $n = 100$ (right).

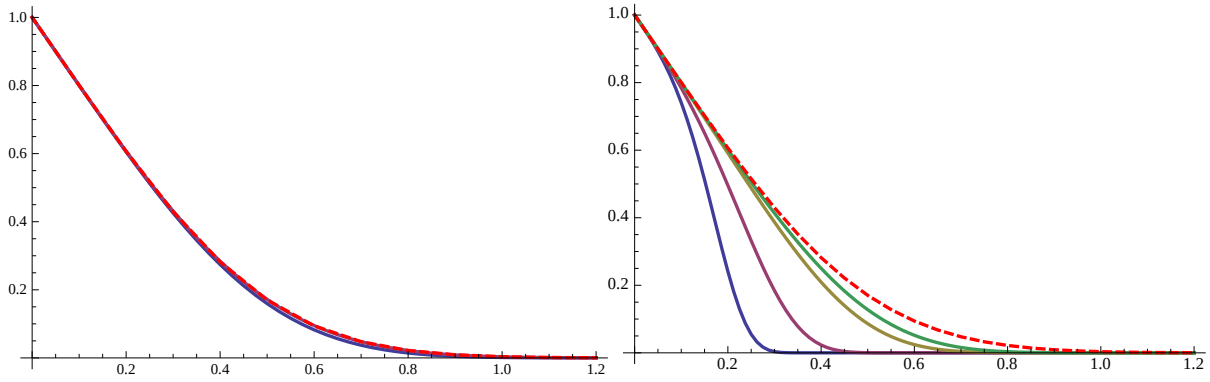

Figure 4: The calculated probability that there are no eigenvalues in the scaled neighbourhood $x + \frac{(-s,s)}{\mathcal{K}_n(x,x)}$ for $n = 50, 100, 200$ and 250 for $x = 1$ (left, $\psi(1) \approx .055$) and $x = 1.5$ (right, $\psi(1.5) \approx .0105$), for the potential $V(x) = \frac{x^2}{5} - \frac{4}{15}x^3 + \frac{x^4}{20} + \frac{8}{5}x$.

orthogonal polynomials using the RH approach. In Figure 3, we plot the gap statistics versus a histogram for the GUE in the interval $(-s, s)$[5].

To see universality in the bulk, we scale the interval with n; in particular, we need to look at the gap probability for

$$\Omega = x + \frac{(-s, s)}{\mathcal{K}_n(x, x)}.$$

Alternatively, $\mathcal{K}_n(x, x)$ can be replaced by its asymptotic distribution to get

$$\Omega = x + \frac{(-s, s)}{n\psi(x)},$$

where $\mathrm{d}\mu = \psi(x)\,\mathrm{d}x$ is the equilibrium measure of V. For x inside the support of μ, this statistic approaches the sine kernel distribution[6]. We demonstrate this in Figure 4 for the degenerate potential, showing that the rate in which the statistics approach universality depends on the magnitude of the density of the equilibrium measure: convergence is more rapid when $\psi(x)$ has larger amplitude.

[5]We are not imposing the bulk scaling introduced below, to demonstrate that the numerical approach does not depend on choosing the scalings correctly.

[6]This was demonstrated in [8, Chapter 8] for an equivalent, rescaled kernel acting on $(-s, s)$. Here, we leave the kernel unmodified, and scale only Ω.

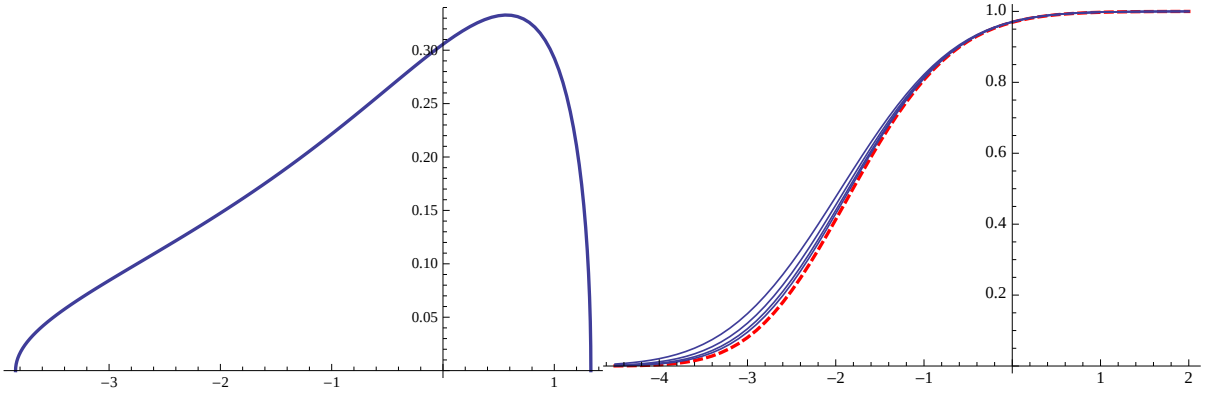

Figure 5: The equilibrium measure for $V(x) = \mathrm{e}^x - x$ (left) and the scaled gap statistic for $n = 10, 20, 40$ and 80 (right). The dashed line is the Tracy–Widom distribution ($n = \infty$).

Next, we consider edge statistics. In the generic position (i.e., when the equilibrium measure has precisely square root decay at its right endpoint b), the gap probability for

$$\Omega = \left(b + \frac{s}{c_V n^{2/3}}, \infty\right)$$

tends to the Tracy–Widom distribution[7]; here c_V is a constant associated with the equilibrium measure, see Section 4.2 for its precise definition and the numerical method for its calculation. In Figure 5, we plot the computed equilibrium measure for $V(x) = \mathrm{e}^x - x$ (computed as described in Section 4.1), and its scaled edge statistic for increasing values of n. While the finite statistics are clearly converging to the Tracy–Widom distribution, the rate of convergence is much slower than the convergence of bulk statistics where the density of the equilibrium measure is large.

Remark There are several methods for calculating universality laws — i.e., $n = \infty$ statistics — including using their Painlevé transcendent representations, see [4] for an overview. An additional approach based on RH problems is to represent, say,

$$\partial_s \log \det(I - \mathcal{S}|_{L^2(-s,s)})$$

as a RH problem. This can be solved numerically for multiple choices of s, and the results integrated numerically, see [7] for examples in the degenerate case. This approach is accurate in the tails, whereas the Fredholm determinant representation that we use only achieves absolute accuracy. However, we are not aware of similar RH problems for finite n.

3 Riemann–Hilbert problems and their numerical solution

Riemann–Hilbert (RH) problems are the fundamental object of study for the remainder of the manuscript, as we will reduce the calculation of orthogonal polynomials to the numerical solution of an RH problem. RH problems are boundary-value problems in the complex plane. One seeks a piecewise-analytic function Φ with specified discontinuities on a given oriented contour Γ. We first define the limits from the left and right of Γ:

[7]We found this particular form by specializing [6, (1.15)], though it is equivalent to the rescaled kernel found in [9, (1.23)].

Definition 1 *Suppose Φ is analytic off an oriented contour Γ. Then, for $s \in \Gamma$, the limit from the positive/left (negative/right) side of Γ is denoted $\Phi^+(s)$ ($\Phi^-(s)$), provided the limit exists and is continuous at s.*

We can now define a RH problem:

Definition 2 *Given an oriented contour Γ and $G : \Gamma \to \mathbb{C}^{2\times 2}$, a RH problem is the task of finding a function $\Phi(z)$ such that*

1. *$\Phi(z)$ is analytic in $\mathbb{C} \setminus \Gamma$,*
2. *$\Phi(z)$ is continuous in $\overline{D}$ for each connected component D of $\mathbb{C} \setminus \Gamma$,*
3. *$\Phi(z)$ satisfies the jump condition*

$$\Phi^+(s) = \Phi^-(s)G(s), \quad s \in \Gamma, \tag{1}$$

4. *and $\lim_{|z|\to\infty} \Phi(z) = I$.*

We use the notation $\Phi = [G; \Gamma]$ when Φ is the unique solution of $[G; \Gamma]$.

Importantly, the RH problems we consider can be converted to equivalent singular integral equations (SIEs) defined on Γ. In this sense, solutions to RH problems are essentially defined by their behaviour at the boundary of their domain of analyticity. While Γ may be complicated and self-intersecting, it is one-dimensional which simplifies the complexity of the problem.

The numerical solution of a RH problem begins with the equivalent SIE as is done in [27]. The starting point for reducing an RH problem to an SIE is the Cauchy transform.

Definition 3 *The Cauchy transform is defined for $z \in \mathbb{C}$ as*

$$\mathcal{C}_\Gamma U(z) = \frac{1}{2\pi \mathrm{i}} \int_\Gamma \frac{U(s)}{s - z} ds.$$

Provided that U is Hölder-continuous — with sufficient decay at infinity when Γ is unbounded — the Cauchy transform is analytic for all z off Γ. Furthermore, its limits from the left and right, denoted $\mathcal{C}_\Gamma^\pm U(s)$ are continuous away from self-intersection and end points of Γ.

We can extend the left and right limits of the Cauchy transform $\mathcal{C}_\Gamma^\pm$ to operators on $L^2(\Gamma)$. These operators satisfy [8, p. 185]:

- *$\mathcal{C}_\Gamma^\pm$ are well-defined bounded linear operators on $L^2(\Gamma)$ and*
- *the Plemelj Lemma holds: $\mathcal{C}_\Gamma^+ - \mathcal{C}_\Gamma^- = I$.*

Before we discuss the numerical method in more detail we make three assumptions:

1. Assume the solution of the given RH problem is of the form

$$\Phi(z) = I + \mathcal{C}_\Gamma U(z), \tag{2}$$

   where $U : \Gamma \to \mathbb{C}^{2\times 2}$ and each entry of U is in $L^2(\Gamma)$.

2. We make an assumption on Γ. Let $\gamma \subset \Gamma$ be the set of self-intersection (junction) points. Assume

- $\Gamma = \Gamma^1 \cup \cdots \cup \Gamma^L$,
- $\Gamma^i \cap \Gamma^j \subset \gamma$, $i \neq j$, and
- $M_j(\Gamma^j) = [-1, 1]$ for an affine transformation $M_j(\Gamma^j)$.

In particular, we assume that Γ is a piecewise-smooth contour.

3. We assume all jump matrices satisfy the product condition:

Definition 4 *For a RH problem $\Phi = [G; \Gamma]$, let $G_j = G|_{\Gamma^j}$ be the restriction of G to Γ^j. For a junction point ζ of Γ, let $\Gamma^1, \ldots, \Gamma^l$ be a counter-clockwise ordering of the subcomponents of Γ that have ζ as an endpoint. G satisfies the product condition if*

$$\prod_{i=1}^{l} G_j^{\sigma_j}(\zeta) = I, \quad \sigma_j = \begin{cases} 1, & \text{if } \Gamma^j \text{ is oriented outwards} \\ -1, & \text{otherwise,} \end{cases}$$

for all junction points ζ of Γ.

A substitution of (2) into (1) while using the Plemelj Lemma yields

$$U - \mathcal{C}_\Gamma^- U(G - I) = G - I. \tag{3}$$

We use the notation

$$\mathcal{C}\,[G; \Gamma]\,U = U - \mathcal{C}_\Gamma^- U(G - I),$$

which defines bounded linear operator on $L^2(\Gamma)$ provided $G \in L^\infty(\Gamma)$.

Our numerical scheme is to solve this SIE using a *collocation method*. We approximate U on each Γ^j by a finite-dimensional sum of *mapped Chebyshev polynomials*:

$$T_k^j(s) = T_k(M_j(s)),$$

where $T_k(x) = \cos(k \arccos x)$ is the kth-order Chebyshev polynomial of the first kind. In general, the order of the approximating polynomial on each Γ^j may be set independently. For simplicity and ease of exposition, we assume all orders are equal. In other words, for $s \in \Gamma$ we approximate $U(s) \approx U_m(s)$, where we define

$$\begin{aligned} U_m(s) &= U_m^j(s) \quad \text{for} \quad s \in \Gamma^j, \qquad \text{where} \\ U_m^j(s) &= \sum_{k=0}^{m-1} U_k^j T_k^j(s), \end{aligned}$$

for as-of-yet unknown coefficients $U_k^i \in \mathbb{C}^{2\times 2}$.

Following the results of [27], if we are given the coefficients, we evaluate $\mathcal{C}\,[G; \Gamma]\,U_m$ *pointwise* by using an exact expression for the Cauchy transform of our basis:

Proposition 1 *[25]*

$$\mathcal{C}_{\Gamma^j} T_k^j(z) = \mathcal{C}_{(-1,1)} T_k(M_j(z))$$

Theorem 1 *[25, 26] Define*

$$\psi_k(z) = \begin{cases} \frac{2}{\pi \mathrm{i}} \operatorname{arctanh} z & \text{for } k = 0 \\ \frac{2}{\pi \mathrm{i}} \frac{-1}{k(1-z^2)}\ {}_2F_1\left(\begin{smallmatrix} 1,\ 1 \\ \frac{3}{2} - (k+1)/2 \end{smallmatrix}; \frac{z^2}{z^2-1} \right) & \text{for } k < 0 \text{ and } k \text{ odd} \\ \frac{2}{\pi \mathrm{i}} \frac{z}{(1-z^2)(1-k)}\ {}_2F_1\left(\begin{smallmatrix} 1,\ 1 \\ \frac{3}{2} - k/2 \end{smallmatrix}; \frac{z^2}{z^2-1} \right) & \text{for } k < 0 \text{ and } k \text{ even} \\ z\psi_{k-1}(z) - \frac{2}{\mathrm{i}\pi k} & \text{for } k > 0 \text{ and } k \text{ odd,} \\ z\psi_{k-1}(z) & \text{for } k > 0 \text{ and } k \text{ even,} \end{cases}$$

where ${}_2F_1$ *is the hypergeometric function [23]. Then*

$$\mathcal{C}T_k(z) \ = -\frac{1}{2}\left[\psi_k(J_+^{-1}(z)) + \psi_{-k}(J_+^{-1}(z))\right],$$

where

$$J_+^{-1}(z) = z - \sqrt{z-1}\sqrt{z+1}$$

is an inverse of the Joukowsky transform $J(z) = \frac{1}{2}(z + z^{-1})$.

We choose the coefficients U_k^j by enforcing (3) to hold pointwise at a collection of Lm points. (Recall that L is the total number of subcontours of Γ.) In other words, we choose points $\left\{z_1^j, \ldots, z_m^j\right\}$ lying on each Γ^j, and solve the $4Lm \times 4Lm$ linear system

$$\mathcal{C}\left[G; \Gamma\right] U_m(z_k^j) = G(z_k^j) - I. \tag{4}$$

We choose *mapped Chebyshev points*:

$$\left\{z_1^j, \ldots, z_m^j\right\} = \left\{ {M_j}^{-1}(-1), {M_j}^{-1}\left(\cos \pi \left[1 - \frac{1}{n-1}\right]\right), \ldots, {M_j}^{-1}(1) \right\}.$$

This means every junction point of Γ is included in the collocation system, with multiplicity equal to the number of contours emanating from the junction point. (We must include these points in the numerical scheme so that $\mathcal{C}U_m$ remains bounded.) We denote these repeated points by

$$\left\{\xi + 0\mathrm{e}^{\mathrm{i}\theta_1}, \ldots, \xi + 0\mathrm{e}^{\mathrm{i}\theta_p}\right\}$$

where $\theta_1, \ldots, \theta_p$ are the angles in which the components of Γ that include ξ as a junction point emanate from ξ. But, as seen in Theorem 1, the Cauchy transform for our basis blows up at such points! To overcome this discrepancy, we assume that the solution satisfies the *zero-sum condition*:

Definition 5 *Let* $\Gamma^{j_1}, \ldots, \Gamma^{j_l}$ *be a counter-clockwise ordering of subcomponents of* Γ *that contain a junction point* ζ *as a endpoint.* U_m *satisfies the zero-sum condition if, at every such junction point it satisfies*

$$\sum_i \sigma_i U_m^{j_i}(\zeta) = 0$$

where $\sigma_i = -1$ *if the left endpoint of* Γ^{j_i} *is* ζ, $\sigma_i = 1$ *if the right endpoint of* Γ^{j_i} *is* ζ.

We define an alternate expression for the Cauchy transform at the junction points by assuming that U_m satisfies the zero-sum condition. Generically, $\mathcal{C}_\Gamma U$ has logarithmic singularities at each junction point of Γ. The zero-sum condition provides a sufficient condition

for $\mathcal{C}_\Gamma U$ to remain bounded as the junction point is approached. An elementary analysis of the Cauchy integral shows that

$$\begin{aligned}\mathcal{C}_{(-1,1)}U(z) &= \frac{1}{2\pi\mathrm{i}}\int_{-1}^{1}\frac{U(s)-U(1)}{s-z}\,\mathrm{d}s + \frac{U(1)}{2\pi\mathrm{i}}\log\left(\frac{z-1}{z+1}\right),\\ &\sim \frac{1}{2\pi\mathrm{i}}\int_{-1}^{1}\frac{U(s)-U(1)}{s-1}\,\mathrm{d}s - \frac{U(1)}{2\pi\mathrm{i}}\log 2\\ &+ \frac{U(1)}{2\pi\mathrm{i}}\left[\log|z-1| + \mathrm{i}\arg(z-1)\right].\end{aligned}$$

The unboundedness of $\mathcal{C}_{(-1,1)}U(z)$ at $z=1$ is a direct consequence of $\log|z-1|$. The zero-sum condition guarantees the cancellation of this term. For a different description of this see [8, p. 185]. Furthermore, it is clear that the value and existence of

$$\lim_{z\to 1}\left[\mathcal{C}_{(-1,1)}U(z) - \frac{U(1)}{2\pi\mathrm{i}}\log|z-1|\right],$$

depends on how $z\to 1$. This motivates a new definition for the Cauchy operators at intersection points, which we express in terms of the mapped Chebyshev basis.

Definition 6 *The finite-part Cauchy transform*[8] $\dashint$ *is defined as follows: For z not an endpoint of Γ^j, it is equivalent to the Cauchy transform:*

$$\dashint_{\Gamma^j} T_k^j(z) = \mathcal{C}_{\Gamma^j} T_k^j(z).$$

Otherwise, for z_L^j the left endpoint of Γ^j and z_R^j the right endpoint, if $\theta\neq\theta_j$ define

$$\begin{aligned}\dashint_{\Gamma^j} T_k^j(z_L^j + 0\mathrm{e}^{\mathrm{i}\theta}) &= a_k^{\mathrm{L}} + \mathrm{i}r_k^{\mathrm{L}}\arg(-\mathrm{e}^{\mathrm{i}(\theta-\theta_j)})\\ \dashint_{\Gamma^j} T_k^j(z_R^j + 0\mathrm{e}^{\mathrm{i}\theta}) &= a_k^{\mathrm{R}} + \mathrm{i}r_k^{\mathrm{R}}\arg(\mathrm{e}^{\mathrm{i}(\theta-\theta_j)})\end{aligned}$$

for (noting that M_j' are constants)

$$\begin{aligned}a_k^{\mathrm{L}} &= (-1)^k\frac{\log 2}{2\pi\mathrm{i}} + \frac{(-1)^k}{\mathrm{i}\pi}\left[\mu_{k-1}(-1)+\mu_k(-1)\right] + r_k^{\mathrm{L}}\log\left|M_j'\right|,\\ a_k^{\mathrm{R}} &= -\frac{\log 2}{2\pi\mathrm{i}} + \frac{1}{\mathrm{i}\pi}\left[\mu_{k-1}(1)+\mu_k(1)\right] + r_k^{\mathrm{R}}\log\left|M_j'\right|,\\ r_k^{\mathrm{L}} &= -\frac{(-1)^k}{2\pi\mathrm{i}} \quad \textit{and} \quad r_k^{\mathrm{R}} = \frac{1}{2\pi\mathrm{i}},\end{aligned}$$

where

$$\mu_k(z) = \sum_{i=1}^{\left\lfloor\frac{k+1}{2}\right\rfloor}\frac{z^{2i-1}}{2i-1}.$$

Corresponding to evaluating on the contour Γ^j itself, define

$$\begin{aligned}\dashint^{\pm}_{\Gamma^j} T_k^j(z_L^j + 0\mathrm{e}^{\mathrm{i}\theta_j}) &= a_k^L \pm \mathrm{i}\pi r_k^L,\\ \dashint^{\pm}_{\Gamma^j} T_k^j(z_R^j + 0\mathrm{e}^{-\mathrm{i}\theta_j}) &= a_k^R \pm \mathrm{i}\pi r_k^R\end{aligned}$$

by the left and right limits as $\theta\to\pm\theta_j$.

[8] Not to be confused with the Hadamard finite-part integral.

The usefulness of this alternative definition is that it is equivalent to the standard Cauchy transform for functions which satisfy the zero-sum condition:

Lemma 1 *[27] If U_m satisfies the zero-sum condition, then*

$$\text{-}\mathcal{C}U_m(z) = \mathcal{C}U_m(z),$$

including limits as z approaches a junction point of Γ.

Sketch of Proof Let ζ be a junction point of Γ. From the asymptotic behaviour of $\operatorname{arctanh} z$, we see near ζ that if ζ is an endpoint of Γ^j ,

$$\mathcal{C}_{\Gamma^j} T_k^j(z) \sim -\frac{\sigma_j}{2\pi \mathrm{i}} \log\left|z - z_L^j\right| + C_{\theta,k}^j$$

where $\theta = \arg(z-\zeta)$ and σ_j is defined as in Definition 5. If ζ is not a junction point of Γ^j, then

$$\mathcal{C}_{\Gamma^j} T_k^j(z) \sim \mathcal{C}_{\Gamma^j} T_k^j(\zeta) =: C_{\theta,k}^j.$$

(where $C_{\theta,k}^i$ is θ independent). Thus,

$$\begin{aligned}\mathcal{C}U_m(z) &= \sum_j \sum_k U_k^j \mathcal{C}_{\Gamma^j} T_k^j(z) \sim -\sum_j \sigma_j U_m^j(\zeta) \frac{1}{2\pi \mathrm{i}} \log\left|z - z_l^j\right| + \sum_j \sum_k C_{\theta,k}^j \\ &= \sum_j \sum_k C_{\theta,k}^j;\end{aligned}$$

since the zero-sum condition ensures that

$$\sum_j \sigma_j U^j(\zeta) = 0.$$

The remaining constant $C_{\theta,k}^j$, which we refer to as the *finite part*, are precisely the constants we defined above. □

Thus, assuming the coefficients U_k^j are in the space so that U_m satisfies the zero-sum condition, we replace (4) by

$$\text{-}\mathcal{C}[G,\Gamma]U_m(z_k^j) = G(z_k^j) - I. \tag{5}$$

This is justified by the following:

Lemma 2 *[27] If the linear system* (5) *is nonsingular, then the calculated U_m satisfies the zero-sum condition.*

Sketch of Proof Let ζ be a junction point, and assume for simplicity that $\sigma_j = 1$ or 0 and Γ_j are ordered by increasing arguments θ_j. Define

$$\Phi_j^{\pm} = I + \text{-}\mathcal{C}^{\pm} U_m(\zeta + 0\mathrm{e}^{\mathrm{i}\theta_j}),$$

and define

$$G_j = G(\zeta + 0\mathrm{e}^{\mathrm{i}\theta_j})$$

(i.e., the limit of the jump along Γ^j). The collocation system imposes $\Phi_j^+ = \Phi_j^- G_j$. But the definition of $\mathcal{C}$ imposes that

$$\Phi_{j+1}^- = \Phi_j^+ + (\theta_{j+1} - \theta_j)S \qquad \text{and} \qquad \Phi_1^- = \Phi_L^+ + (\theta_1 + 2\pi - \theta_L)S$$

for

$$S = -\sum_j \sigma_j \frac{U_j(0)}{2\pi \mathrm{i}}.$$

These equations give

$$\begin{aligned}\Phi_L^+ &= \Phi_L^+ G_1 \cdots G_L + S\left[(\theta_1 + 2\pi - \theta_L) G_1 \cdots G_L + \sum_{j=2}^{L} (\theta_j - \theta_{j-1}) G_i \cdots G_L\right] \\ &= \Phi_L^+ + S\left[(\theta_1 + 2\pi - \theta_L) I + \sum_{j=2}^{L} (\theta_j - \theta_{j-1}) G_j \cdots G_L\right]\end{aligned}$$

where we use the product condition (see Definition 4) satisfied by the jump matrix of the RH problem:

$$G_1 \cdots G_L = I.$$

If

$$(\theta_1 + 2\pi - \theta_L) I + \sum_{j=2}^{L} (\theta_j - \theta_{j-1}) G_j \cdots G_L$$

is nonsingular (the *nonsingular junction condition*), then $S = 0$, implying the zero-sum condition.

Now suppose the nonsingular junction condition is not satisfied, and we replace the condition in the collocation system that

$$\Phi_L^+ = \Phi_L^- G_L,$$

with $S = 0$. We then have

$$\Phi_{j+1}^- = \Phi_j^+ \quad \text{and} \quad \Phi_1^- = \Phi_L^+.$$

Thus

$$\begin{aligned}\Phi_L^- G_L &= \Phi_{L-1}^+ G_{L-1} G_L = \cdots = \Phi_{L-1}^+ G_1 \cdots G_{L-1} G_L \\ &= \Phi_L^+,\end{aligned}$$

and the removed condition is still satisfied. In other words, the two linear systems are *equivalent*.

□

In conclusion, the fact that the linear system is nonsingular implies that the numerically constructed

$$\Phi_m(z) = I + \mathcal{C} U_m(z)$$

is analytic off Γ, bounded on $\mathbb{C}$ and satisfies the correct jumps at the collocation points.

3.1 Function spaces

Before we continue we must briefly introduce some notions and notation that allow issues related to regularity to be addressed. We follow [28] and interpret the finite-dimensional operator defined by applying $\mathcal{C}[G;\Gamma]$ to a piecewise polynomial then sampling and interpolating the resulting function at $\{z_k^j\}$ as mapping of piecewise polynomials to piecewise polynomials. Indeed, the sampled function at the values $\{z_k^j\}$ is identified with its unique

piecewise-polynomial interpolant and we use $\mathcal{I}_m$ to denote this interpolation operator. Define $L^2_m(\Gamma^j)$ to be the space of matrix-valued functions with entries being mapped mth order polynomials. For $\Gamma = \Gamma^1 \cup \cdots \cup \Gamma^L$ define

$$L^2_m(\Gamma) = \bigoplus_{j=1}^{L} L^2_m(\Gamma^j).$$

Define $L^2_{m,z}(\Gamma)$ to be the closed subspace of $L^2_m(\Gamma)$ consisting of functions that satisfy the zero-sum condition. Thus $\mathcal{I}_m \mathcal{C}[G;\Gamma]$ is a well-defined linear operator from $L^2_{m,z}(\Gamma)$ to $L^2_m(\Gamma)$. As is mentioned in [28], $\mathcal{I}_m \mathcal{C}[G;\Gamma]$ maps to a proper subspace $\tilde{L}^2_m(\Gamma)$ of $L^2_m(\Gamma)$. Note that this is required since $L^2_{m,z}(\Gamma)$ is necessarily of lower dimension than $L^2_m(\Gamma)$.

For each component contour Γ^j and $k \in \mathbb{N}^+$ we define the Sobolev spaces $H^k(\Gamma^j)$ and $W^{k,\infty}(\Gamma^j)$ in the usual way [28]. For the contour Γ

$$H^k(\Gamma) = \bigoplus_{j=1}^{L} H^k(\Gamma_j), \quad W^{k,\infty}(\Gamma) = \bigoplus_{j=1}^{L} W^{k,\infty}(\Gamma^j).$$

Finally, for Banach spaces X, Y we use $\mathcal{L}(X,Y)$ to denote the Banach space of bounded linear operators from X to Y with the induced operator norm. If $X = Y$ then $\mathcal{L}(X,Y) = \mathcal{L}(X)$.

3.2 Uniform approximation theory

Since we are interested in the behaviour of orthogonal polynomials for all n, including the onset of universality as n becomes large, we look for a method that retains accuracy for arbitrarily large n. To accomplish this, we will utilize the uniform approximation framework developed in [28].

The building blocks of uniform approximation consist of a strategy for solving RH problems, and a theorem for showing uniform approximation:

1. Assumption 1: Assume that the numerical method used for solving RH problems satisfies a reasonable conditioning property.
2. Lemma 3: Truncate unbounded jump matrices when they are close to the identity.
3. (9): Separate and scale contours near stationary points (using Assumption 2 as a guide).
4. Lemma 4: Iteratively solve the separated contours, recovering the solution to the original RH problem.
5. Theorem 2: Reduce proving uniform approximation to showing boundedness of jump matrices and inverse operators of the resulting RH problems.

For our numerical scheme to fit into the uniform approximation framework, we must assume the following:

Assumption 1 *Assume there exists a constant $\alpha > 0$ such that*

$$\|(\mathcal{I}_m \mathcal{C}[G;\Gamma])^{-1}\|_{\mathcal{L}(Y_m, X_m)} \leq D m^{\alpha} \|\mathcal{C}[G;\Gamma]^{-1}\|_{\mathcal{L}(L^2(\Gamma))}, \quad D > 0,$$
$$X_m = L^2_{m,z}(\Gamma), \quad Y_m = \tilde{L}^2_m(\Gamma),$$

whenever $\mathcal{C}[G;\Gamma]$ is invertible, $G - I \in W^{1,\infty} \cap H^1(\Gamma)$ and G satisfies the production condition.

Determining α for the numerical method in [27] is still an open problem but numerical tests indicate that it holds true for all $\alpha > 0$. Under this assumption it is shown in [28] that

$$\|U - U_m\|_{L^2(\Gamma)} \leq Cm^{2+\alpha-k}\|U\|_{H^k(\Gamma)},$$

where C depends only on $\mathcal{C}[G;\Gamma]$ and its inverse. As before, U is the solution of $\mathcal{C}[G;\Gamma]U = G - I$ and U_m is its numerical approximation. When U depends on the parameter n, the degree of the orthogonal polynomial, we aim to bound $\|U\|_{H^k(\Gamma)}$ uniformly in n for sufficiently large k. The uniform approximation theory provides a framework to do exactly this. We demonstrate the essentials with an example.

Problem 1 *For $c > 0$ and $n \geq 1$, consider the scalar RH problem*

$$\begin{aligned} &\Phi^+(z) = \Phi^-(z)\left(1 + \frac{1}{2}e^{-n(z-a)^2+\mathrm{i}cn}\right), \quad z \in \mathbb{R} \\ &\Phi(\infty) = 1. \end{aligned} \tag{6}$$

While this problem can be solved in terms of explicit integrals we study it from our numerical analysis point-of-view. The first step is truncation:

Lemma 3 (Contour truncation [28]) *Assume $G - I \in W^{k,\infty} \cap H^k(\Gamma)$. Then for every $\epsilon > 0$ there exists an matrix-valued function G_ϵ, $G_\epsilon - I \in W^{k,\infty} \cap H^k(\Gamma)$, and a bounded contour Γ_ϵ such that*

- *$G_\epsilon = I$ on $\Gamma \setminus \Gamma_\epsilon$,*
- *$G = G_\epsilon$ in a neighbourhood of every intersection point of Γ,*
- *$\|G_\epsilon - G\|_{L^2\cap L^\infty(\Gamma)} < \epsilon$, and*
- *$\|\mathcal{C}[G;\Gamma] - \mathcal{C}[G_\epsilon;\Gamma_\epsilon]\|_{\mathcal{L}(L^2(\Gamma))} < \epsilon\|\mathcal{C}_\Gamma^-\|_{\mathcal{L}(L^2(\Gamma))}$.*

This justifies the truncation of the contour $\mathbb{R}$ to an interval while introducing a small error. Furthermore, this truncation can be done to preserve the smoothness of the solutions. In practice, we ignore the issues related to smoothness and we truncate the contour when the jump is, to machine precision, unity (or the identity matrix) since that is our numerical limitation.

For $n = 1$ it suffices to truncate $\mathbb{R}$ to $\Gamma = [-7 + a, 7 + a]$. We deal with $n > 1$ with the next step: scaling. Define k through $z = k/\sqrt{n} + a$ and define $\Gamma_n = [-7, 7]/\sqrt{n} + a$. We approximate (6) with

$$\begin{aligned} &\Psi^+(z) = \Psi^-(z)\left(1 + \frac{1}{2}e^{-n(z-a)^2+\mathrm{i}cn}\right), \quad z \in \Gamma_n \\ &\Psi(\infty) = 1. \end{aligned} \tag{7}$$

We change to the k variable. Define $\tilde{\Psi}(k) = \Psi(k/\sqrt{n} + a)$ so that

$$\begin{aligned} &\tilde{\Psi}^+(z) = \tilde{\Psi}^-(z)\left(1 + \frac{1}{2}e^{-k^2+\mathrm{i}cn}\right), \quad k \in [-7, 7] \\ &\tilde{\Psi}(\infty) = 1. \end{aligned} \tag{8}$$

When this problem is treated numerically the convergence rate (as $m \to \infty$) to the solution does not depend on n.

The additional complication that arises in applications is that the contours consist of multiple components. To generalize the scaling approach, assume that we have a sequence of RH problems $\{[G_n;\Gamma_n]\}_n$ depending on the parameter n. The theory of [28] requires that Γ_n can be decomposed into l components which are scaled individually:

$$\Gamma_n = \Omega_n^1 \cup \cdots \cup \Omega_n^l, \tag{9}$$

where $\{\Omega_n^j\}_{j=1}^l$ are mutually disjoint and have the form

$$\Omega_n^j = \alpha_n^j \Omega^j + \beta^j.$$

In other words, we assume Γ_n is the disjoint union of contours, each of which is an affine transformation of a fixed contour. Once we have this separation of Γ_n we attempt to solve the RH problem $[G_n;\Gamma_n]$ in an iterative way. Define the restricted jumps $G_n^j = G_n|_{\Omega_n^j}$ and the jumps after variable change $H_n^j(k) = G_n^j(\alpha_n^j k+\beta^j)$, $k \in \Omega_j$. The following result is found in [28]. For notational simplicity we suppress the dependence on n. But it is important to note in the general case every function, but not Ω^j, depends on n.

Lemma 4 (Scaled and shifted solver) *Define* $\tilde{\Phi}_1 = [H^1;\Omega^1]$ *and* $\Phi_1 = \tilde{\Phi}_1\left(\frac{z-\beta^1}{\alpha^1}\right)$. *Furthermore, for each* $j = 2,3,\ldots,l$ *define* $\Phi_{i,j}(k) = \Phi_i(\alpha^j k + \beta^j)$ *and set*

$$\tilde{\Phi}_j = \left[\Phi_{j-1,j}\cdots\Phi_{1,j}H_j\Phi_{1,j}^{-1}\cdots\Phi_{j-1,j}^{-1};\Omega^j\right], \quad \Phi_j(z) = \tilde{\Phi}_j\left(\frac{z-\beta^j}{\alpha^j}\right).$$

Then $\Phi = \Phi_1\cdots\Phi_l$ *solves* $[G_n;\Gamma_n]$.

This lemma states that we can treat each disjoint contour separately. We first solve a RH problem on one subcomponent of Γ_n and modify the full RH problem by the solution. This removes the subcomponent from the RH problem and modifies the remaining jumps. This process is repeated until all contours are taken account of.

We use the following rule of thumb to determine the proper scalings α_n^j (compare with Problem 1):

Assumption 2 *If the jump matrix* G *has a factor* $e^{n\theta}$ *and* β^j *corresponds to a* q*th order stationary point (*i.e., $\theta(z) \sim C(z-\beta^j)^q$*), then the scaling which achieves asymptotic stability is (a constant multiple of)* $\alpha_n^j = n^{-1/q}$.

3.3 Conditions for uniform approximation

A significant question is whether each of these smaller RH problems $[H_j;\Omega^j]$ is solvable. From a practical numerical standpoint this possible issue does not seem to affect the conditioning of the method. From a theoretical standpoint this question is settled for large n in [28] provided $\alpha_n^j \to 0$ for all j as $n \to \infty$. We make a necessary assumption that is true in all cases we consider here, after possible truncation.

Assumption 3 *Assume that the jump matrix* G *is* C^∞ *when restricted to each component* Γ^j *of* Γ *and decays to the identity matrix faster than any polynomial at each isolated endpoint of* Γ *and at* ∞ *if* $\infty \in \Gamma$.

The following theorem is the fundamental result of [28] and gives the required tools to address the accuracy of the Riemann–Hilbert numerical methods for orthogonal polynomials for arbitrarily large n:

Theorem 2 *Assume*

- $\mathcal{C}[H_n^j, \Omega^j]^{-1}$ *exists and the norm* $\|\mathcal{C}[H_n^j, \Omega^j]^{-1}\|_{\mathcal{L}(L^2(\Omega^j))} \leq C$ *for all* j *and* n,
- $\|H_n^j\|_{W^{k,\infty}(\Omega^j)} \leq C_k$ *for all* j *and* n, *and*
- $\alpha_n^j \to 0$ *as* $n \to \infty$.

Then for n *sufficiently large*

- *The algorithm of Lemma 4 has solutions at each stage,*
- *The approximation* U_m^j *of* U^j *— the solution of the SIE at stage* j *in the algorithm of Lemma 4 — converges uniformly with* n *in the* L^2 *norm as* $m \to \infty$.

The theorem states that if the contours Ω_n^j all have decaying measure then local boundedness properties of functions and operators on each of the contours is made global for n large. As is demonstrated below, bounding the $W^{k,\infty}$ norms of the matrices H_n^j is often straightforward and the boundedness properties of the inverse operator follows from the asymptotic analysis of the RH problem.

Remark Similar results hold when the bounds in Theorem 2 are known for a 'nearby' RH problem. In this case bounds on the nearby RH problem give slightly weaker convergence properties that can still be seen to be uniform in an appropriate sense [28].

Remark An important aspect of this theory is that whether or not the theory applies in a straightforward way is not critical. The theory still guides deformation, truncation and scaling of contours.

4 Orthogonal polynomials

To calculate the kernel $\mathcal{K}_n$, we need to calculate the polynomials $\pi_n(x)$ and $\gamma_{n-1}\pi_{n-1}(x)$, where $\pi_0(x), \pi_1(x), \ldots$ are monic polynomials orthogonal to the weight $\mathrm{e}^{-nV(x)}\,\mathrm{d}x$, supported on the real line. These polynomials can be expressed in terms of the solution to a RH problem:

Problem 2 *[17] The function*

$$Y(z) = \begin{pmatrix} \pi_n(z) & \mathcal{C}_{\mathbb{R}}[\pi_n \mathrm{e}^{-nV}](z) \\ -2\pi\mathrm{i}\gamma_{n-1}\pi_{n-1}(z) & -2\pi\mathrm{i}\gamma_{n-1}\mathcal{C}_{\mathbb{R}}[\pi_{n-1}\mathrm{e}^{-nV}](z) \end{pmatrix},$$

where

$$\gamma_{n-1} = \left[\int \pi_{n-1}^2(x)\mathrm{e}^{-nV(x)}\,\mathrm{d}x\right]^{-1}$$

solves the RH problem on the real line

$$Y^+ = Y^- \begin{pmatrix} 1 & \mathrm{e}^{-nV(x)} \\ 0 & 1 \end{pmatrix} \qquad \textit{and} \qquad Y \sim \begin{pmatrix} z^n & 0 \\ 0 & z^{-n} \end{pmatrix} \quad \textit{as} \quad z \to \infty.$$

To apply the numerical method described in Section 3, we must transform the RH problem for Y into a suitable form for numerical solution. To accomplish this, we transform Y by representing it explicitly in terms of new functions which satisfy the following properties:

1. $Y \mapsto T$ **so that** $T \sim I$ **at infinity:** (Eq. (11)) The condition at infinity is necessary for the representation

$$T(z) = I + \mathcal{C}_\Gamma U(z), \tag{10}$$

to be valid. Furthermore, this representation is necessary for the application of the chosen collocation method.

2. $T \mapsto S$ **so that the oscillatory jumps of** T **are transformed to exponentially decaying jumps of** S**:** (Eq. (12)) Oscillations in the jump matrix are an indication of an oscillatory solution. In this case the solution is difficult to resolve numerically. Thus, we seek exponential decay to resolve the complication.

3. $S \mapsto \Phi$ **so that the jumps of** Φ **are localized and scaled:** (Eq. (13)) The uniform approximation theory is applicable when the RH problem has localized and scaled jump contours. This is the step that produces accurate numerical results for arbitrarily large n.

4.1 Equilibrium measures

Our first task is to remove the growth in Y at ∞. To accomplish this, we must compute the so-called g-function, which has logarithmic growth at infinity so that $\mathrm{e}^{\pm ng(z)} \sim z^{\pm n}$, but has special jump properties so that its incorporation into the RH problem will allow for uniform approximation.

The g function is associated with the equilibrium measure of V:

Definition 7 *The equilibrium measure* μ *is the minimizer of*

$$\iint \log \frac{1}{|x-y|} \,\mathrm{d}\mu(x)\,\mathrm{d}\mu(y) + \int V(x)\,\mathrm{d}\mu(x).$$

We review the numerical approach to calculating equilibrium measures in [24], but in the context of calculating the g-function. For simplicity, we assume that the equilibrium measure of V is supported on a single interval (a, b); a sufficient condition is that V is convex [8]. (We remark that the below procedure was adapted to the multiple interval case in [24], and adapting our numerical procedure for computing orthogonal polynomials, and thence invariant ensemble statistics, to such cases would be straightforward.)

With the correct choice of (a, b), there exists g satisfying the following scalar RH problem:

1. g analytic off $(-\infty, b)$ and g' is bounded at a and b,
2. $g_+(x) + g_-(x) = V(x) - \ell$ for $a \le x \le b$ and some constant ℓ,
3. $g(z) \sim \log z + \mathcal{O}\left(\frac{1}{z}\right) \quad \text{as} \quad z \to \infty$, and
4. $g_+(x) - g_-(x) = 2\pi\mathrm{i}$ for $-\infty < x < a$.

To calculate g, we first calculate its derivative $\phi = g'$, which satisfies:

1. ϕ is analytic off (a, b) and is bounded at a and b,
2. $\phi_+(x) + \phi_-(x) = V'(x)$ for $a \le x \le b$,
3. $\phi(z) \sim \frac{1}{z} \quad \text{as} \quad z \to \infty$.

(Differentiating the asymptotics at infinity is justified because $g - \log z$ has an isolated singular point at infinity at which it is bounded; therefore it is analytic at infinity.) In typical analysis, ϕ is defined as an integral (a Cauchy transform). For computational purposes, it is preferable to use the following representation in terms of the Chebyshev expansion of V'.

Given a candidate (a, b), we describe all functions that have the correct jump on (a, b), decay at infinity and have weaker than pole singularities at a and b.

Definition 8 *Let $\chi \in \mathbb{C}$ and*

$$f(x) = \sum_{k=0}^{\infty} f_k T_k(x),$$

where T_k is the kth order Chebyshev polynomial of the first kind. Define

$$\mathcal{P}_\chi f(z) = \sum_{k=0}^{\infty} f_k J_+^{-1}(z)^k - \frac{f_0}{2} \frac{z}{\sqrt{z-1}\sqrt{z+1}} + \frac{\chi}{\sqrt{z-1}\sqrt{z+1}},$$

for the inverse Joukowski transform

$$J_+^{-1}(z) = z - \sqrt{z-1}\sqrt{z+1}.$$

Denote the affine map from (a, b) to $(-1, 1)$ as

$$M_{(a,b)}(z) = \frac{a+b}{2} + \frac{b-a}{2} z$$

and define

$$\mathcal{P}_{(a,b),\chi} f(z) = \mathcal{P}_\chi [f \circ M_{(a,b)}](M_{(a,b)}^{-1}(z)).$$

Theorem 3 *[25, 24] Suppose the Chebyshev expansion of $f(M_{(a,b)}(x))$ converges absolutely. Then, for all $\chi \in \mathbb{C}$, $\mathcal{P}_{(a,b),\chi} f(z)$ is a solution to*

$$\phi_+(x) + \phi_-(x) = f(x) \quad \text{for} \quad x \in (a, b) \quad \text{and} \quad \phi(\infty) = 0.$$

Furthermore, every solution to this scalar RH problem that has weaker singularities than poles at a and b is equal to $\mathcal{P}_{(a,b),\chi} f(z)$ for some χ.

Sketch of Proof We sketch the proof for $(a, b) = (-1, 1)$. The fact that (directly verifiable by the substitution $x = \cos\theta$)

$$T_k(x) = \frac{J_\downarrow^{-1}(x)^k + J_\downarrow^{-1}(x)^{-k}}{2},$$

where

$$J_\downarrow^{-1}(x) = x - \mathrm{i}\sqrt{1-x}\sqrt{1+x} = \lim_{\epsilon \downarrow 0} J_+^{-1}(x + \mathrm{i}\epsilon)$$

implies that $\mathcal{P}_\chi f$ satisfies the correct jumps (using absolute convergence of the series to interchange limits).

Now suppose $\tilde{\phi}$ also satisfies

$$\tilde{\phi}_+(x) + \tilde{\phi}_-(x) = f(x) \quad \text{for} \quad x \in (-1, 1) \qquad \text{and} \qquad \tilde{\phi}(\infty) = 0$$

with weaker than pole singularities at ± 1. Then $\kappa = \mathcal{P} f - \tilde{\phi}$ satisfies

$$\kappa_+(x) + \kappa_-(x) = 0 \quad \text{for} \quad x \in (-1, 1).$$

If we let $\delta(z) = \kappa(z)\sqrt{z-1}\sqrt{z+1}$, we have $\delta_+ = \delta_-$, i.e., δ is continuous (and thus analytic) on $(-1,1)$. Because κ has weaker than pole singularities at ± 1, we have that δ also has weaker than pole singularities at ± 1. Since these singularities are isolated, it follows that δ is analytic at ± 1, and hence analytic everywhere: δ is constant. This shows that κ is a constant multiple of $\frac{1}{\sqrt{z-1}\sqrt{z+1}}$, completing the proof.

□

Based on the preceding theorem we want to choose (a,b) and χ so that $\phi = \mathcal{P}_{(a,b),\chi}[V']$. So that ϕ has the correct properties, we need to investigate the Chebyshev coefficients of

$$V'(M_{(a,b)}(x)) = \sum_{k=0}^{\infty} V_k T_k(x).$$

To achieve the desired properties, we want ϕ to be bounded:

$$V_0 = 0 \qquad \text{and} \qquad \chi = 0.$$

We also want $\phi(z) \sim \frac{1}{z}$:

$$\frac{b-a}{8} V_1 = 1.$$

These two conditions give us a function

$$F(a,b) = \begin{pmatrix} V_0 \\ (b-a)V_1 - 8 \end{pmatrix},$$

for which we want to find a root. We calculate V_0 and V_1 to high accuracy using the composite trapezoidal rule applied to

$$\int_{-1}^{1} \frac{V'(M_{(a,b)}(x))T_k(x)}{\sqrt{1-x^2}}\,\mathrm{d}x = -2\int_{-\pi}^{\pi} V'(M_{(a,b)}(\cos\theta))\cos k\theta\,\mathrm{d}\theta.$$

This calculation is trivially differentiable with respect to a and b, hence we easily apply Newton iteration to find a root of F. Convexity ensures that this root is unique [24].

Once (a,b) are computed, we calculate $\phi(z)$ by using the discrete cosine transform to calculate the Chebyshev coefficients of V'. We then have the equilibrium measure [24]

$$\mathrm{d}\mu = \frac{\mathrm{i}}{2\pi}\left[\phi^+(x) - \phi^-(x)\right]\,\mathrm{d}x = \frac{\sqrt{1 - M_{(a,b)}^{-1}(x)^2}}{2\pi} \sum_{k=1}^{\infty} V_k U_{k-1}(M_{(a,b)}^{-1}(x))\,\mathrm{d}x$$

where U_k are the Chebyshev polynomials of the second kind. This expression comes from Plemelj's lemma and the fact that ϕ is the Cauchy transform of $\mathrm{d}\mu$:

$$\phi(z) = \frac{1}{2\pi\mathrm{i}} \int \frac{\mathrm{d}\mu(x)}{x-z}.$$

To calculate g, we compute an indefinite integral of ϕ that has the correct decay at infinity [24]:

$$g(z) = \int^z \phi(z)\,\mathrm{d}z = \frac{b-a}{4}\left[V_1\left(\frac{J_+^{-1}(M_{(a,b)}^{-1}(z))^2}{2} - \log J_+^{-1}(M_{(a,b)}^{-1}(z))\right) + \sum_{k=2}^{\infty} V_k\left(\frac{J_+^{-1}(M_{(a,b)}^{-1}(z))^{k+1}}{k+1} - \frac{J_+^{-1}(M_{(a,b)}^{-1}(z))^{k-1}}{k-1}\right)\right].$$

This formula was derived by mapping $J_+^{-1}(M_{(a,b)}^{-1}(z))$ back to the unit circle, where it became a trivially integrable Laurent series. Choosing (arbitrarily) $x \in (a,b)$, we calculate

$$\ell = V(x) - g_+(x) - g_-(x).$$

The numerically calculated g consists of approximating V_k using the discrete Cosine transform and truncating the sum. Due to the analyticity of V, the errors in these computed coefficients are negligible, and the approximation of g is uniformly accurate in the complex plane.

4.2 Scaling constant for edge statistics

Associated with the equilibrium measure are the *Mhaskar–Rakhmanov–Saff numbers* [22, 31] c_V — along with the analytically unneeded $d_V = b - c_V$ — which we need to know to determine the correct scaling so that the edge statistics tend to the Tracy–Widom distribution. We re-express the constant c as stated in [9] in terms of constants that we have already calculated: the support of the equilibrium measure and its Chebyshev coefficients. The equilibrium measure for the scaled potential $V(M_{(a,b)}(x))$ has support $(-1,1)$. Its equilibrium measure is

$$\begin{aligned} {M_{(a,b)}}'(x)\psi(M_{(a,b)}(x))\,\mathrm{d}x &= \frac{b-a}{2}\psi(M_{(a,b)}(x))\,\mathrm{d}x = (b-a)\frac{\sqrt{1-x^2}}{4\pi}\sum_{k=1}^{\infty} V_k U_{k-1}(x)\,\mathrm{d}x \\ &= \frac{\sqrt{1-x^2}}{2\pi}h(x)\,\mathrm{d}x, \end{aligned}$$

as in [9, (3.3)]. We define the constant

$$\alpha = \left(\frac{h(1)^2}{2}\right)^{1/3} = \frac{1}{2}\left[(b-a)\sum_{k=1}^{\infty} kV_k\right]^{2/3}$$

as in [9, (3.10)]. The scaling constant is then

$$c_V = \frac{2\alpha}{b-a} = (b-a)^{-1/3}\left[\sum_{k=1}^{\infty} kV_k\right]^{2/3}.$$

Remark For the degenerate potential of Figure 4, $c = 0$ and hence the scaling breaks down. This coincides with the fact that the edge statistics for the associated ensemble does not follow the standard Tracy–Widom distribution.

4.3 Lensing the RH problem

We rewrite Y to normalize the behaviour at infinity:

$$Y = \begin{pmatrix} \mathrm{e}^{\frac{n\ell}{2}} & 0 \\ 0 & \mathrm{e}^{-\frac{n\ell}{2}} \end{pmatrix} T \begin{pmatrix} \mathrm{e}^{-ng} & 0 \\ 0 & \mathrm{e}^{ng} \end{pmatrix} \begin{pmatrix} \mathrm{e}^{-\frac{n\ell}{2}} & 0 \\ 0 & \mathrm{e}^{\frac{n\ell}{2}} \end{pmatrix}, \tag{11}$$

so that $T \sim I$ and has a jump along the real line, on which it satisfies

$$T_+ = T_- \begin{pmatrix} \mathrm{e}^{n(g_- - g_+)} & \mathrm{e}^{n(g_+ + g_- + \ell - V)} \\ 0 & \mathrm{e}^{n(g_+ - g_-)} \end{pmatrix}$$

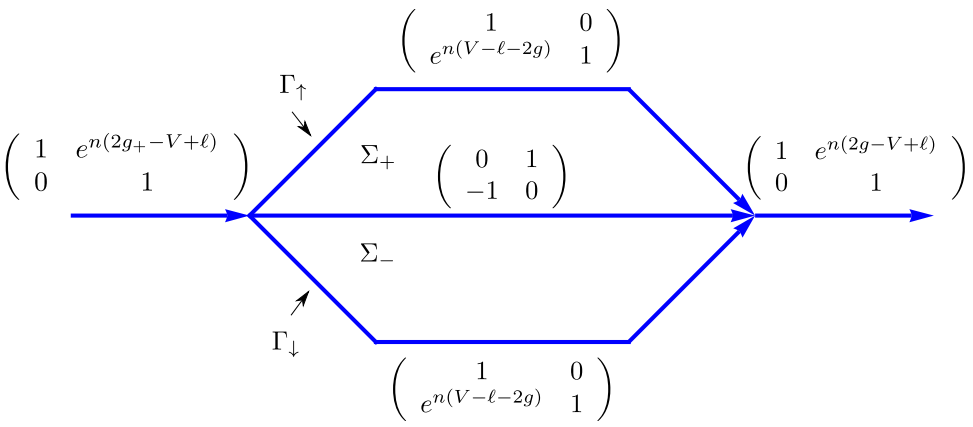

Figure 6: The jumps of S.

$$= T_- \begin{cases} \begin{pmatrix} 1 & \mathrm{e}^{n(g_+ + g_- + \ell - V)} \\ 0 & 1 \end{pmatrix} & x < a \\ \begin{pmatrix} \mathrm{e}^{n(g_- - g_+)} & 1 \\ 0 & \mathrm{e}^{n(g_+ - g_-)} \end{pmatrix} & a < x < b \\ \begin{pmatrix} 1 & \mathrm{e}^{n(2g+\ell-V)} \\ 0 & 1 \end{pmatrix} & b < x \end{cases}$$

We appeal to properties of equilibrium measures [8, (7.57)] to assert that

$$g_+(x) + g_-(x) + \ell - V < 0$$

for $x < a$ and $x > b$, thus those contributions of the jump matrix are isolated around a and b. On the other hand, $g_+ - g_-$ is imaginary between a and b [8, pp. 195], hence $\mathrm{e}^{\pm n(g_+ - g_-)}$ becomes increasingly oscillatory on (a, b). We wish to deform the RH problem into the complex plane to convert oscillations into exponential decay. To accomplish this, we introduce the lensing as in Figure 6, where we rewrite T by

$$T(z) = S(z) \begin{cases} \begin{pmatrix} 1 & 0 \\ \mathrm{e}^{n(V-\ell-2g)} & 1 \end{pmatrix} & z \in \Sigma_+ \\ \begin{pmatrix} 1 & 0 \\ \mathrm{e}^{n(V-\ell-2g)} & 1 \end{pmatrix} & z \in \Sigma_- \\ I & \text{otherwise.} \end{cases} \tag{12}$$

By substituting

$$g_+ = V - g_- - \ell,$$

we see that the oscillations have been removed completely from supp μ:

$$\begin{aligned} S_+ &= T_+ \begin{pmatrix} 1 & 0 \\ -\mathrm{e}^{n(V-\ell-2g_+)} & 1 \end{pmatrix} = T_+ \begin{pmatrix} 1 & 0 \\ -\mathrm{e}^{n(g_- - g_+)} & 1 \end{pmatrix} \\ &= T_- \begin{pmatrix} \mathrm{e}^{n(g_- - g_+)} & 1 \\ 0 & \mathrm{e}^{n(g_+ - g_-)} \end{pmatrix} \begin{pmatrix} 1 & 0 \\ -\mathrm{e}^{n(g_- - g_+)} & 1 \end{pmatrix} \\ &= T_- \begin{pmatrix} 0 & 1 \\ -1 & \mathrm{e}^{n(g_+ - g_-)} \end{pmatrix} = S_- \begin{pmatrix} 1 & 0 \\ -\mathrm{e}^{n(V-\ell-2g_-)} & 1 \end{pmatrix} \begin{pmatrix} 0 & 1 \\ -1 & \mathrm{e}^{n(V-\ell-2g_-)} \end{pmatrix} \\ &= S_- \begin{pmatrix} 0 & 1 \\ -1 & 0 \end{pmatrix}. \end{aligned}$$

However, we have introduced new jumps on $\Gamma_\uparrow$ and $\Gamma_\downarrow$, on which

$$S_+ = T_+ = T_- = S_- \begin{pmatrix} 1 & 0 \\ \mathrm{e}^{n(V-\ell-2g)} & 1 \end{pmatrix}.$$

4.4 Removing the connecting jump

We have successfully converted oscillations to exponential decay. However, to maintain accuracy of the numerical algorithm for large n, we must isolate the jumps to neighbourhoods of the endpoints a and b. To achieve this, we remove the jump along (a, b). We introduce a *parametrix* that solves the RH problem exactly on this single contour. In other words, we require a function which satisfies the following RH problem:

$$N_+(x) = N_-(x) \begin{pmatrix} 0 & 1 \\ -1 & 0 \end{pmatrix} \qquad \text{for} \qquad a < x < b \qquad \text{and} \qquad N(\infty) = I.$$

The solution is [8]

$$N(z) = \frac{1}{2\nu(z)} \begin{pmatrix} 1 & \mathrm{i} \\ -\mathrm{i} & 1 \end{pmatrix} + \frac{\nu(z)}{2} \begin{pmatrix} 1 & -\mathrm{i} \\ \mathrm{i} & 1 \end{pmatrix} \quad \text{for} \quad \nu(z) = \left(\frac{z-b}{z-a} \right)^{1/4};$$

i.e., $\nu(z)$ is a solution to

$$\nu_+(x) = \mathrm{i}\nu_-(x) \quad \text{for} \quad a < x < b \qquad \text{and} \qquad \nu(\infty) = 1.$$

An issue with using N as a parametrix is that it introduces singularities at a and b, hence we also introduce local parametrices to avoid these singularities. In the event that the equilibrium measure $\psi(x)$ has exactly *square root decay* at the edges, asymptotically accurate local parametrices are known (see Section 5.1). However, if the equilibrium measure has higher order decay (*à la* the higher-order Tracy–Widom distributions [6]), the asymptotically accurate local parametrices are only known in terms of a RH problem.

For numerical purposes, however, we do not need the parametrix to be asymptotically accurate: we achieve asymptotic accuracy by scaling the contours. Thus we introduce the *trivially constructed* local parametrices which satisfy the jumps of S in neighbourhoods of a and b:

$$P_a(z) = \begin{pmatrix} \begin{cases} \begin{pmatrix} 1 & 0 \\ 1 & 1 \end{pmatrix} & \frac{\pi}{3} < \arg(z-a) < \pi \\ \begin{pmatrix} 1 & -1 \\ 1 & 0 \end{pmatrix} & -\pi < \arg(z-a) < -\frac{\pi}{3} \\ \begin{pmatrix} 0 & -1 \\ 1 & 0 \end{pmatrix} & -\frac{\pi}{3} < \arg(z-a) < 0 \\ I & \text{otherwise} \end{cases} \end{pmatrix} \begin{pmatrix} \mathrm{e}^{n(V-\ell-2g)} & 0 \\ 0 & \mathrm{e}^{-n(V-\ell-2g)} \end{pmatrix}$$

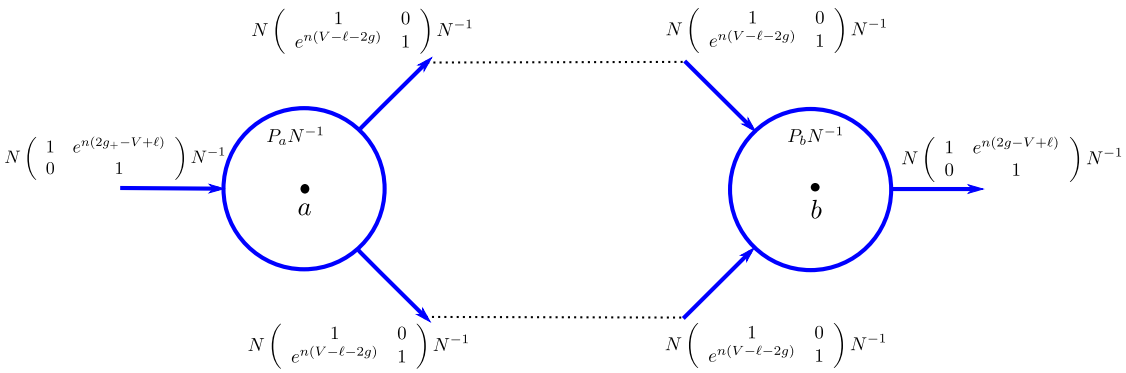

Figure 7: The jumps of Φ. We use a counter-clockwise orientation on the circle about a and b.

and

$$P_b(z) = \left(\begin{cases} \begin{pmatrix} 1 & 0 \\ -1 & 1 \end{pmatrix} & \frac{2\pi}{3} < \arg(z-b) < \pi \\ \begin{pmatrix} 0 & -1 \\ 1 & 1 \end{pmatrix} & -\pi < \arg(z-b) < -\frac{2\pi}{3} \\ \begin{pmatrix} 1 & -1 \\ 0 & 1 \end{pmatrix} & -\frac{2\pi}{3} < \arg(z-b) < 0 \\ I & \text{otherwise} \end{cases} \right) \begin{pmatrix} \mathrm{e}^{n(V-\ell-2g)} & 0 \\ 0 & \mathrm{e}^{-n(V-\ell-2g)} \end{pmatrix}.$$

We write

$$S(z) = \Phi(z) \begin{cases} N(z) & |z-a| > r \text{ and } |z-b| > r \\ P_b(z) & |z-b| < r \\ P_a(z) & |z-a| < r \end{cases} \tag{13}$$

The final RH problem for Φ satisfies the jumps depicted in Figure 7. Note that, in general, r will depend on n. We discuss this in more detail in the next section.

In practice, we do not use infinite contours. We truncate contours when the jump matrix is, to machine precision, the identity matrix (see Lemma 3). In all cases we consider here, after proper deformations the jump matrices are C^∞ smooth and are exponentially decaying to the identity matrix for large z. We deform the remaining contours to be line segments connecting their endpoints. The resulting jump contour consists only of affine transformations of the unit interval.

4.5 Contour scalings

In the case of a non-degenerate equilibrium measure, $V(z)-\ell-2g(z) \sim c_a(z-a)^{3/2}$ as $z \to a$ and $V(z) - \ell - 2g \sim c_b(z-b)^{3/2}$ as $z \to b$. In accordance with Assumption 2, we scale the contours like $n^{-2/3}$:

$$\Omega_n^1 = -n^{-2/3}\Omega^0 + a \qquad \text{and} \qquad \Omega_n^2 = n^{-2/3}\Omega^0 + b,$$

where the Ω^0 that is used in practice is depicted in the left graph of Figure 8, and the angle of the contours are chosen to match the direction of steepest descent. This implies that $r \sim n^{-2/3}$. In the first-order degenerate case (eg., $V(x) = \frac{x^2}{5} - \frac{4}{15}x^3 + \frac{x^4}{20} + \frac{8}{5}x$),

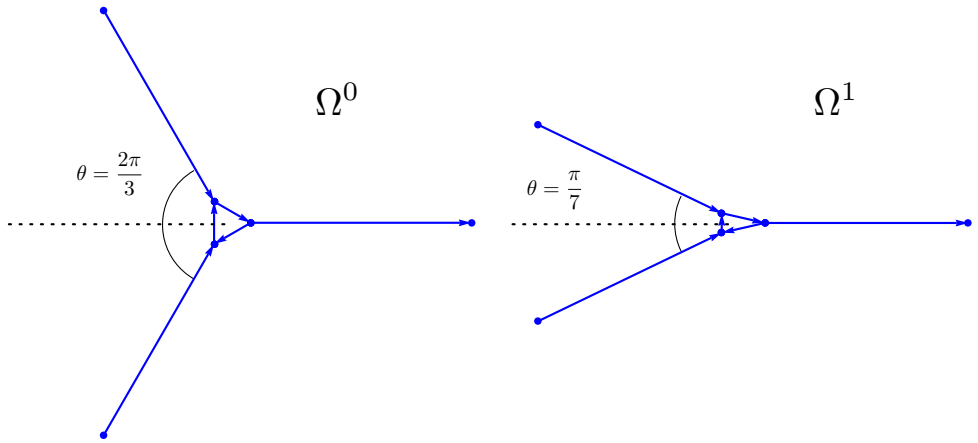

Figure 8: The pre-scaled Ω^0 used for non-degenerate endpoints and the pre-scaled Ω^1 used for first-order degenerate endpoints. These are the contours that are used in practice.

$V(z) - \ell - 2g(z) \sim c_b(z-b)^{7/2}$ as $z \to b$ and so we scale like $n^{-7/2}$ (implying $r \sim n^{-7/2}$) at the degenerate endpoint:

$$\Omega_n^1 = n^{-2/3}\Omega^0 + a \qquad \text{and} \qquad \Omega_n^2 = n^{-7/2}\Omega^1 + b,$$

where Ω^1 is depicted in the right graph of Figure 8 (the angle is sharper to attach to the new direction of steepest descent). Higher-order degenerate equilibrium measures require higher-order scalings, but this can be determined systematically by investigating the number of vanishing derivatives of the equilibrium measure. This is the final form of the RH problem that we used in the numerical calculations of Section 2. A discussion the accuracy of the numerical solution of this scaled and shifted RH problem for large n is presented below.

5 Achieving uniform approximation

Having described the form of the RH problem which we solve numerically, we want to show that the resulting approximation remains accurate as n becomes large by satisfying the conditions of Theorem 2. While we do not use the local parametrix in the numerical algorithm, we do need it to show that the deformed contour satisfies the uniform approximation properties. Thus we introduce the local parametrix in Section 5.1, noting that it can also be used in the numerical scheme to achieve uniform approximation (though not for degenerate potentials). We then use this parametrix to show uniform approximation properties in Section 5.2. To achieve this, we must adapt the jump matrix to cancel the effects of singularities resulting from the parametrix $N(z)$.

5.1 The classical Airy parametrix

In this section we present the deformation and asymptotic solution of the RH problem, needed for the asymptotic analysis of orthogonal polynomials, as in [8, Section 7.6]. For brevity of presentation in this section we only consider potentials of the form $V(x) = x^{2m}$. For the asymptotic analysis and deformations in the more general case of $V(x)$ polynomial see [10, 11, 12, 13].

The goal of the section is to construct a parametrix $\hat{\Phi}$ that is a sectionally analytic, matrix-valued function so that $S\hat{\Phi}^{-1} \to I$ as $n \to \infty$ where S is the solution the deformed

and lensed RH problem in Figure 6. The RH problem for the error $E = S\hat{\Phi}^{-1}$ has smooth solutions and is a near-identity RH problem in the sense that the associated singular integral operator is expressed in the form $I - K_n$ with $\|K_n\|_{\mathcal{L}(L^2)} \to 0$ as $n \to \infty$. Thus E can be computed via a Neumann series for sufficiently large n.

The deformation proceeds much in the same way as Section 4.4, except we have $a = -c$, $b = c$ for $c > 0$ [8]. We replace P_a and P_b with new functions ψ_{-c} and ψ_c that are constructed out of the Airy function. It is important to note that due to the near-identity nature of the problem we do not scale the jump contour (i.e., $r \sim 1$). We now construct the functions ψ_{-c} and ψ_c. As an intermediate step, define

$$\Psi(s) = \begin{cases} \begin{pmatrix} \mathrm{Ai}\,(s) & \mathrm{Ai}\,(\omega^2 s) \\ \mathrm{Ai}\,'(s) & \omega^2 \mathrm{Ai}\,(\omega^2 s) \end{pmatrix} e^{-i\frac{\pi}{6}\sigma_3} & 0 < \arg s < \frac{2\pi}{3} \\ \begin{pmatrix} \mathrm{Ai}\,(s) & \mathrm{Ai}\,(\omega^2 s) \\ \mathrm{Ai}\,'(s) & \omega^2 \mathrm{Ai}\,'(\omega^2 s) \end{pmatrix} e^{-i\frac{\pi}{6}} & \frac{2\pi}{3} < \arg s < \pi \\ \begin{pmatrix} \mathrm{Ai}\,(s) & \mathrm{Ai}\,(\omega^2 s) \\ \mathrm{Ai}\,'(s) & \omega^2 \mathrm{Ai}\,'(\omega^2 s) \end{pmatrix} e^{-i\frac{\pi}{6}\sigma_3} \begin{pmatrix} 1 & 0 \\ -1 & 1 \end{pmatrix} & \pi < \arg s < \frac{4\pi}{3} \\ \begin{pmatrix} \mathrm{Ai}\,(s) & -\omega^2 \mathrm{Ai}\,(\omega s) \\ \mathrm{Ai}\,'(s) & -\mathrm{Ai}\,'(\omega s) \end{pmatrix} e^{-i\frac{\pi}{6}\sigma_3} \begin{pmatrix} 1 & 0 \\ 1 & 1 \end{pmatrix} & \frac{4\pi}{3} < \arg s < 2\pi \end{cases},$$

$\omega = e^{\frac{2\pi i}{3}}$.

The relations

$$\mathrm{Ai}\,(s) + \omega \mathrm{Ai}\,(\omega s) + \omega^2 \mathrm{Ai}\,(\omega^2 s) = 0,$$
$$\mathrm{Ai}\,'(s) + \omega^2 \mathrm{Ai}\,'(\omega s) + \omega \mathrm{Ai}\,'(\omega^2 s) = 0,$$

can be used to show that $\Psi(s)$ satisfies the following jump conditions

$$\Psi^+(s) = \Psi^-(s) \begin{cases} \begin{pmatrix} 1 & 1 \\ 0 & 1 \end{pmatrix} & s \in \gamma_1 \\ \begin{pmatrix} 1 & 0 \\ 1 & 1 \end{pmatrix} & s \in \gamma_2 \\ \begin{pmatrix} 0 & 1 \\ -1 & 0 \end{pmatrix} & s \in \gamma_3 \\ \begin{pmatrix} 1 & 0 \\ 1 & 1 \end{pmatrix} & s \in \gamma_4 \end{cases}.$$

See Figure 9 for $\gamma_i,\ i = 1, \ldots 4$.

Since we only consider V even in this section, the equilibrium measure is supported on a symmetric interval $[-c, c]$ for $c > 0$. Define

$$\Lambda(z) = \frac{3}{2}\varphi(z)(z-c)^{-3/2}, \quad \lambda(z) = (z-c)(\Lambda(z))^{2/3},$$
$$\varphi(z) = \frac{1}{2}\left(V(z) - \ell\right) - g(z).$$

It follows from the branching properties of φ that Λ and λ are analytic in a neighbourhood of c. Furthermore, since $\lambda(c) = 0$ and $\lambda'(c) = (\Lambda(c))^{2/3} \neq 0$ we use it as a conformal change of variables mapping a neighbourhood of $z = c$ into a neighbourhood of the origin. More precisely, fix an $\epsilon > 0$ and define $O_c = \lambda^{-1}(\{|z| < \epsilon\})$.

Define

$$\psi_c(z) = L(z)\Psi(n^{2/3}\lambda(z))e^{n\varphi(z)\sigma_3},$$
$$L(z) = \begin{pmatrix} 1 & -1 \\ -i & -i \end{pmatrix} \sqrt{\pi} e^{i\frac{\pi}{6}} n^{\sigma_3/6} ((z+c)\Lambda^{2/3}(z))^{\sigma_3/4}.$$

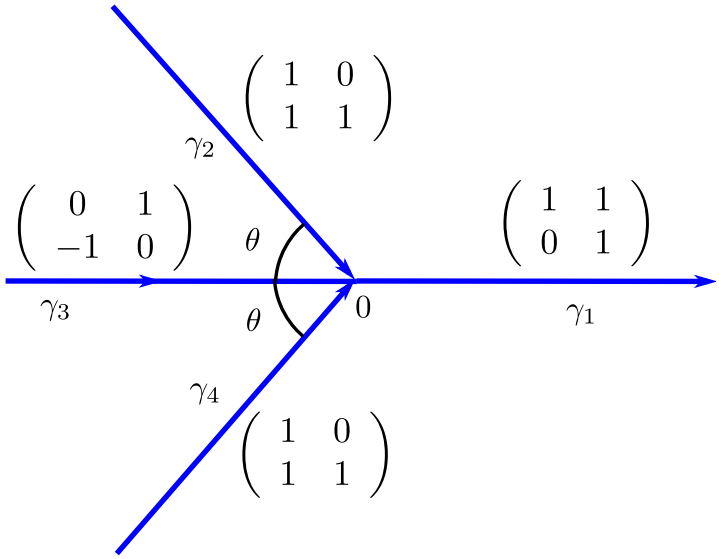

Figure 9: The jump contours for Ψ with jump matrices. We use $\theta = 2\pi/3$ below.

ψ_c solves the local RH problem shown in Figure 10(b). The symmetry of $V(x)$ implies that $\psi_{-c}(z) = \sigma_3\psi_c(-z)\sigma_3$ satisfies the jumps shown in Figure 10(a). We are ready to define the full parametrix

$$\hat{\Phi}(z) = \begin{cases} \psi_c(z) & z \in O_c \\ \psi_{-c}(z) & z \in -O_c \\ N(z) & \text{otherwise} \end{cases}. \tag{14}$$

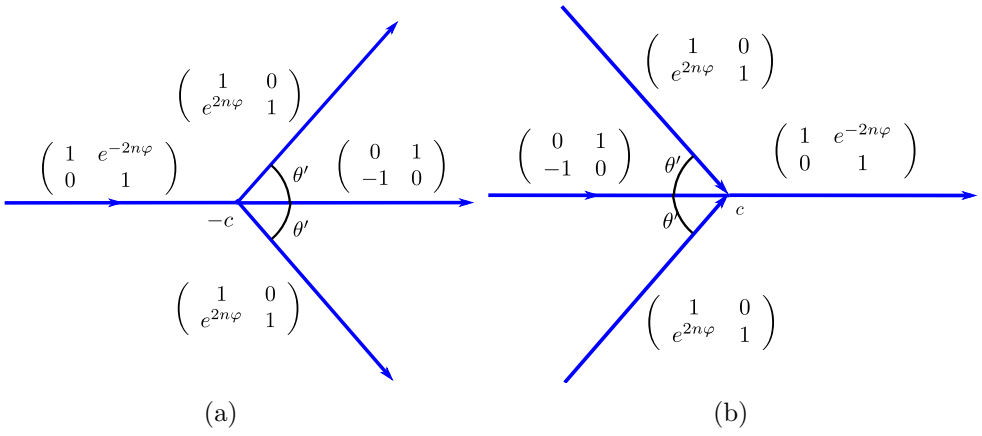

Figure 10: The local parametrices near $z = \pm c$. As above $\theta' > 0$ is included for concreteness but its exact value is not needed. (a) The jump contours for ψ_{-c} with jump matrices. (b) The jump contours for ψ_c with jump matrices.

We need a result concerning the asymptotics of the Airy function

$$\begin{aligned} \mathrm{Ai}\,(s) &= \frac{1}{2\sqrt{\pi}} s^{-1/4} e^{-\frac{2}{3}s^{3/2}} \left(1 + \mathcal{O}\left(\frac{1}{s^{3/2}}\right)\right), \\ \mathrm{Ai}\,'(s) &= -\frac{1}{2\sqrt{\pi}} s^{3/4} e^{-\frac{2}{3}s^{3/2}} \left(1 + \mathcal{O}\left(\frac{1}{s^{3/2}}\right)\right), \end{aligned}$$

as $s \to \infty$ and $|\arg s| < \pi$. These asymptotics, along with the definition of $\lambda(z)$, can be used

to show

$$\psi_c(z)N^{-1}(z) = I + \mathcal{O}(n^{-1}), \quad z \in \partial O_c, \tag{15}$$
$$\psi_{-c}(z)N^{-1}(z) = I + \mathcal{O}(n^{-1}), \quad z \in \partial O_{-c}, \tag{16}$$

as $n \to \infty$ uniformly in z provided $O_c \cup O_{-c}$ is contained in a sufficiently narrow strip containing the real line. See [8, Section 7.6] for the details.

We take the RH problem for S in Figure 6 and label ∂O_c and ∂O_{-c}. Note that without loss of generality we take O_c and O_{-c} to be open balls around c and $-c$, respectively. (Analyticity allows us to deform any open, simply connected set containing c or $-c$ to a ball.)

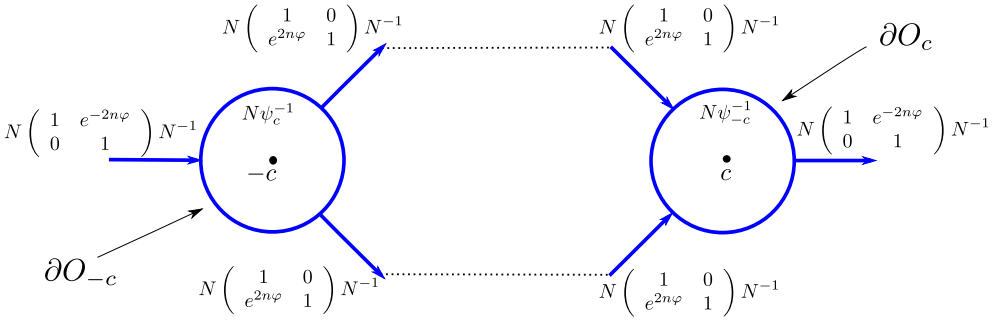

Figure 11: The jump contours Ω for the error E. The jump matrix J for E which is taken as the piecewise definition as shown. We use a counter-clockwise orientation for the circles about $\pm c$. These circles have radius $r \sim 1$.

Since ψ_c and ψ_{-c} solve the RH problem locally in O_c and O_{-c}, respectively, the function $E = S\hat{\Psi}^{-1}$ is analytic in O_c and O_{-c}. See Figure 11 for the jump contour, Ω, and jump matrix, J, for the RH problem for E. It is shown in [8, Section 7.6] using (15) that the jump matrix for this RH problem tends uniformly to the identity matrix as $n \to \infty$, again provided that all contours are in sufficiently small neighbourhood of the real line. Thus

$$\| I - \mathcal{C}\left[J; \Omega\right] \|_{\mathcal{L}(L^2(\Omega))} = \mathcal{O}(n^{-1}),$$

and a Neumann series produces the unique solution u of $\mathcal{C}\left[J; \Omega\right] u = J - I$. S is found via the expression

$$S(z) = (I + \mathcal{C}_\Omega u(z))\hat{\Psi}(z).$$

5.2 Obtaining the bounds in Theorem 2

To apply Theorem 2 one has to first identify the correct scalings for the contours and second, establish bounds on the relevant operator norms and function derivatives.

5.2.1 The RH problem for E

In this case, we consider numerically solving the RH problem for E, rather than scaling and shifting the contours as we do in practice. This simplifies the proof of uniform approximation considerably though the exact form of the Airy parametrix is needed explicitly in the numerics. Unfortunately, this local parametrix does not apply to degenerate potentials. We contrast this with the analysis in the following section where the Airy parametrix is needed to prove asymptotic accuracy but is in no way needed to perform calculations.

Take $\Gamma_n = \Omega$ (see (9)); that is, we do not scale the contour. The near-identity nature of the RH problem allows us to avoid any scaling of the problem. Using the asymptotic expansions for the derivatives of Airy functions one can show that

$$\|J - I\|_{W^{k,\infty}(\Omega)\cap H^k(\Omega)} = \mathcal{O}(n^{-1}).$$

Furthermore, the fact that $\|\mathcal{C}[J;\Omega]^{-1}\|_{\mathcal{L}(L^2(\Omega))} < C$ follows easily from the Neumann series argument already given. Therefore Theorem 2 shows that the numerical method will uniformly approximate solutions of this RH problem for small and arbitrarily large n.

To demonstrate the convergence properties of the solution for large n we use the following procedure. Let U_m denote the approximation of u obtained using the numerical method for RH problems discussed above with m collocation points per contour. When we break up Ω into both its non-self-intersecting components and into its components that can be represented by affine transformations of the unit interval we end up with 14 contours. Thus, we use a total of $14m$ collocation points. We solve the RH problem with $m = 10$ and then again with $m = 20$. We sample U_{10} at each collocation point for U_{20} and measure the maximum difference at these collocations points. We define this difference to be the *Cauchy error*. Figure 12 demonstrates that the error decreases as $n \to \infty$.

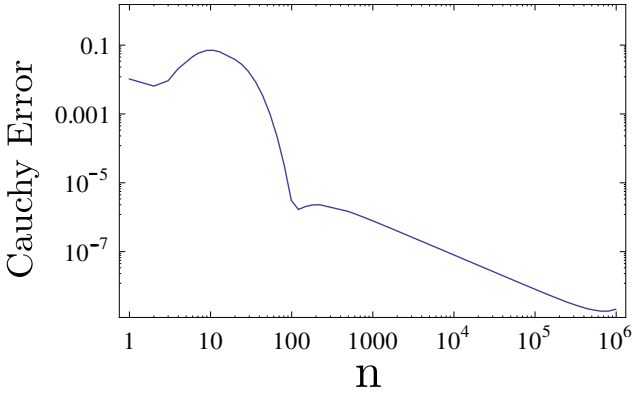

Figure 12: The *Cauchy error* between U_{10} and U_{20} as $n \to \infty$. This plot indicates that it takes fewer collocation points to approximate E as n increases.

5.2.2 The RH problem for Φ

While for non-degenerate potentials we can solve the RH problem associated with E numerically, the RH problem for Φ that we use in practice is of a fundamentally simpler form. No additional special functions (e.g Airy functions) are needed and yet the contours are located away from the stationary points, a and b (we return, for now, to allowing general potentials). All deformations are performed by a reordering and analytic continuation of previously defined functions. Thus we want to show that our strategy of scaling contours does indeed satisfy the criteria of uniform approximation of Theorem 2.

To achieve uniform approximation, we must first alter the jump matrix so that it remains bounded as $n \to \infty$. This will be achievable using only properties of $N(z)$ near a and b, and we prove the resulting jump matrix is bounded in Lemma 7. We also need to show that the inverse of the operator is bounded. Using the local parametrix, we accomplish this in Lemmas 5 and 6.

In this section we assume we are in the non-degenerate case. (While we claim that uniform approximation is indeed achievable for degenerate potentials, proving this would

be more challenging due to lack of explicit local parametrices.) We therefore consider the following jump contour (see Figure 13)

$$\Gamma_n = \Omega_n^1 \cup \Omega_n^2,$$

for

$$\Omega_n^1 = n^{-2/3}\Omega^0 + a \qquad \text{and} \qquad \Omega_n^2 = n^{-2/3}\Omega^0 + b.$$

Furthermore, define G to be the jump matrix for Φ, see Figure 7.

We first rectify the issue with the jumps on these scaled contours: as $n \to \infty$, they approach the unbounded singularities of $N(z)$, violating the condition of Theorem 2 that jump matrix must be bounded. However, we expand

$$\begin{aligned}
N(a+zn^{-2/3}) &= \frac{n^{1/6}}{2}\left(\frac{b-a}{z}\right)^{\frac{1}{4}}\begin{pmatrix}1 & -\mathrm{i}\\ \mathrm{i} & 1\end{pmatrix} + \frac{n^{-1/6}}{2(b-a)}\left(\frac{b-a}{z}\right)^{\frac{3}{4}}\begin{pmatrix}1 & \mathrm{i}\\ -\mathrm{i} & 1\end{pmatrix} + \mathcal{O}\left(n^{-\frac{1}{2}}\right),\\
N(a+zn^{-2/3})^{-1} &= \frac{n^{1/6}}{2}\left(\frac{b-a}{z}\right)^{\frac{1}{4}}\begin{pmatrix}1 & \mathrm{i}\\ -\mathrm{i} & 1\end{pmatrix} + \frac{n^{-1/6}}{2(b-a)}\left(\frac{b-a}{z}\right)^{\frac{3}{4}}\begin{pmatrix}1 & -\mathrm{i}\\ \mathrm{i} & 1\end{pmatrix} + \mathcal{O}\left(n^{-\frac{1}{2}}\right),\\
N(b+zn^{-2/3}) &= \frac{n^{1/6}}{2}\left(\frac{b-a}{z}\right)^{\frac{1}{4}}\begin{pmatrix}1 & \mathrm{i}\\ -\mathrm{i} & 1\end{pmatrix} + \frac{n^{-1/6}}{2(b-a)}\left(\frac{b-a}{z}\right)^{\frac{3}{4}}\begin{pmatrix}1 & -\mathrm{i}\\ \mathrm{i} & 1\end{pmatrix} + \mathcal{O}\left(n^{-\frac{1}{2}}\right),\\
N(b+zn^{-2/3})^{-1} &= \frac{n^{1/6}}{2}\left(\frac{b-a}{z}\right)^{\frac{1}{4}}\begin{pmatrix}1 & -\mathrm{i}\\ \mathrm{i} & 1\end{pmatrix} + \frac{n^{-1/6}}{2(b-a)}\left(\frac{b-a}{z}\right)^{\frac{3}{4}}\begin{pmatrix}1 & \mathrm{i}\\ -\mathrm{i} & 1\end{pmatrix} + \mathcal{O}\left(n^{-\frac{1}{2}}\right).
\end{aligned}$$

Define

$$\bar{N}_{a,n} = n^{-1/6}\begin{pmatrix}1 & -\mathrm{i}\\ \mathrm{i} & 1\end{pmatrix} + n^{1/6}\begin{pmatrix}1 & \mathrm{i}\\ -\mathrm{i} & 1\end{pmatrix}$$

and

$$\bar{N}_{b,n} = n^{-1/6}\begin{pmatrix}1 & \mathrm{i}\\ -\mathrm{i} & 1\end{pmatrix} + n^{1/6}\begin{pmatrix}1 & -\mathrm{i}\\ \mathrm{i} & 1\end{pmatrix}$$

so that

$$N(a+zn^{-2/3})\bar{N}_{a,n}, \quad \bar{N}_{a,n}^{-1}N(a+zn^{-2/3})^{-1}, \quad N(b+zn^{-2/3})\bar{N}_{b,n} \quad \text{and} \quad \bar{N}_{b,n}^{-1}N(b+zn^{-2/3})^{-1}$$

are uniformly bounded for z restricted to an annulus around zero as $n \to \infty$. These matrices are used to remove the growth of the jump matrix in the limit $n \to \infty$. We demonstrate this procedure, which is a modification of the algorithm in Lemma 4. We truncate the contours of the RH problem for Φ by removing the dashed contours in Figure 7. For $\epsilon > 0$ and small, this gives us an approximation Φ_ϵ of Φ with jump matrix G_ϵ so that $G_\epsilon - I$ is supported on $\Omega_n^1 \cup \Omega_n^2$. Additionally, G_ϵ satisfies

$$\|N^{-1}G_\epsilon N - N^{-1}GN\|_{L^2\cap L^\infty} = \mathcal{O}(\epsilon) \text{ and } G_\epsilon(z) = G(z) \text{ for } |z-a| = r \text{ or } |z-b| = r. \quad (17)$$

Our method of scaling contours ensures that ϵ is independent of n. We separate the RH problem for Φ_ϵ into two problems $[G_1;\Omega_n^1]$ and $[G_2;\Omega_n^2]$ with solutions Φ_1 and Φ_2, respectively. See Figure 13 for the piecewise definition of G_1 and G_2. Our solution procedure is (formally) as follows:

1. Scale G_1: Define $H_1(z) = G_1(b+zn^{-2/3})$.
2. Remove the growth of $H_1(z)$: If $\hat{\Phi}_1 = [H_1;\Omega_0]$ define

$$\bar{\Phi}_1(z) = \begin{cases} \bar{N}_{b,n}\hat{\Phi}_1\bar{N}_{b,n}^{-1}(z) & \text{if } z > rn^{2/3},\\ \bar{N}_{b,n}\hat{\Phi}_1 & \text{if } z < rn^{2/3}. \end{cases} \quad (18)$$

A straightforward calculation shows that $\bar{\Phi}_1^+(z) = \bar{\Phi}^-(z)\bar{H}_1(z)$ where

$$\bar{H}_1(z) = \begin{cases} \bar{N}_{b,n} H_1(z) \bar{N}_{b,n}^{-1} & \text{if } |z| > rn^{2/3}, \\ H_1(z)\bar{N}_{b,n}^{-1}, & \text{if } |z| = rn^{2/3}. \end{cases}$$

Recall that in this case the contour is scaled according to $r \sim n^{-2/3}$.

3. Solve for $\bar{\Phi}_1 = [\bar{H}_1; \Omega_0]$ and therefore

$$\Phi_1 = [G_1; \Omega_n^1] = \bar{N}_{b,n}^{-1} \bar{\Phi}_1 \left(n^{2/3}(z-b) \right) \bar{N}_{b,n}.$$

4. Modify G_2: If $\Phi_\epsilon = [G_\epsilon; \Gamma_n]$ then $\Phi_\epsilon \Phi_1^{-1}$ has the jump $\tilde{G}_2 = \Phi_1 G_2 \Phi_1^{-1}$ on Ω_n^2 and is analytic elsewhere.

5. Scale $\tilde{G}_2$: Define $\tilde{H}_2(z) = \tilde{G}_2(a + zn^{-2/3})$.

6. Remove the growth of $\tilde{H}_2(z)$: As in (18), define

$$\bar{\Phi}_2(z) = \begin{cases} \bar{N}_{a,n} \tilde{\Phi}_2 \bar{N}_{a,n}^{-1}(z) & \text{if } z > rn^{2/3}, \\ \bar{N}_{a,n} \tilde{\Phi}_2 & \text{if } z < rn^{2/3}. \end{cases}$$

where $\tilde{\Phi}_2 = [\tilde{H}_2; \Omega_0]$. Then $\bar{\Phi}_2^+(z) = \bar{\Phi}_2^-(z)\bar{H}_2(z)$ where

$$\bar{H}_2(z) = \begin{cases} \bar{N}_{a,n} \tilde{H}_2(z) \bar{N}_{a,n}^{-1} & \text{if } |z| > rn^{2/3}, \\ \tilde{H}_2(z)\bar{N}_{a,n}^{-1}, & \text{if } |z| = rn^{2/3}. \end{cases}$$

7. Solve for $\bar{\Phi}_2 = [\bar{H}_2; \Omega_0]$ and therefore

$$\Phi_2 = [\tilde{G}_2; \Omega_n^1] = \bar{N}_{a,n}^{-1} \bar{\Phi}_2 \left(n^{2/3}(z-a) \right) \bar{N}_{a,n}.$$

8. $\Phi = [G; \Gamma_n] = \Phi_1 \Phi_2$.

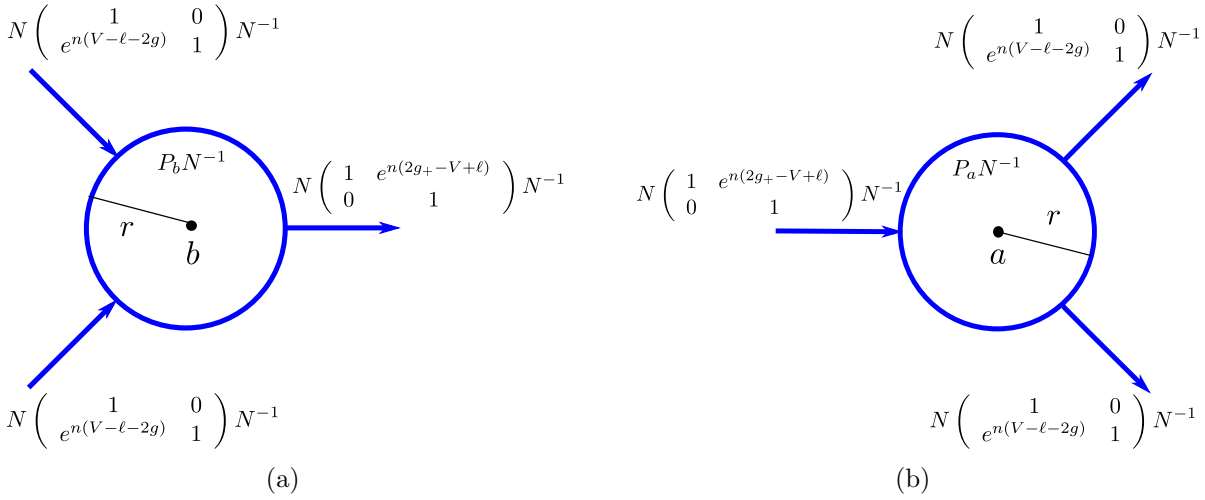

Figure 13: The separate RH problems for Φ_1 and Φ_2. All circles have counter-clockwise orientation. (a) The jump contour Ω_n^1 and jump matrices for Φ_1. (b) The jump contour Ω_n^2 and jump matrices for Φ_2.

We solve two RH problems in this procedure and it is seen that the RH problems have jump matrices that are uniformly bounded in n. This is a necessary condition (but not

sufficient!) for the numerical method to be asymptotically accurate. To further analyse the asymptotic behaviour of these RH problems we must bound the inverse of the operators by comparing the solutions with the Airy parametrix. We assume again that $V(x) = x^{2m}$ so that we have $a = -c$ and $b = c$, $c > 0$. We use this restriction for convenience: we have already defined the parametrix associated with this choice of V above.

We must alter our local parametrices to investigate their behaviour both on the fixed outer contour ∂O_c and the scaled contour of the RH problem on which we solve numerically. Therefore, we alter the local parametrices by defining (compare with (13))

$$\Psi_{-c}(z) = \begin{cases} \psi_{-c}(z)P^{-1}_{a=-c}(z) & \text{if } |z+c| < r, \\ \psi_{-c}(z)N^{-1} & \text{if } |z+c| > r \text{ and } z \in O_{-c}, \\ I, & \text{otherwise,} \end{cases}$$

$$\Psi_{c}(z) = \begin{cases} \psi_{c}(z)P^{-1}_{b=c}(z) & \text{if } |z-c| < r, \\ \psi_{c}(z)N^{-1} & \text{if } |z-c| > r \text{ and } z \in O_{c}, \\ I, & \text{otherwise.} \end{cases}$$

The jump contours Ω_n^c and Ω_n^{-c} for the RH problems for Ψ_c and Ψ_{-c} with jump matrices J_c and J_{-c} are shown in Figure 14.

The following lemmas present a step toward our final result that proves asymptotic accuracy: they demonstrate that the local parametrices Ψ_c and Ψ_{-c} can be used to bound operator inverses. For the analysis, we extend G_1 (G_2) to Ω_n^c (Ω_n^{-c}) by defining $G_1 = I$ on $\Omega_n^c \setminus \Omega_n^1$ ($G_2 = I$ on $\Omega_n^{-c} \setminus \Omega_n^2$).

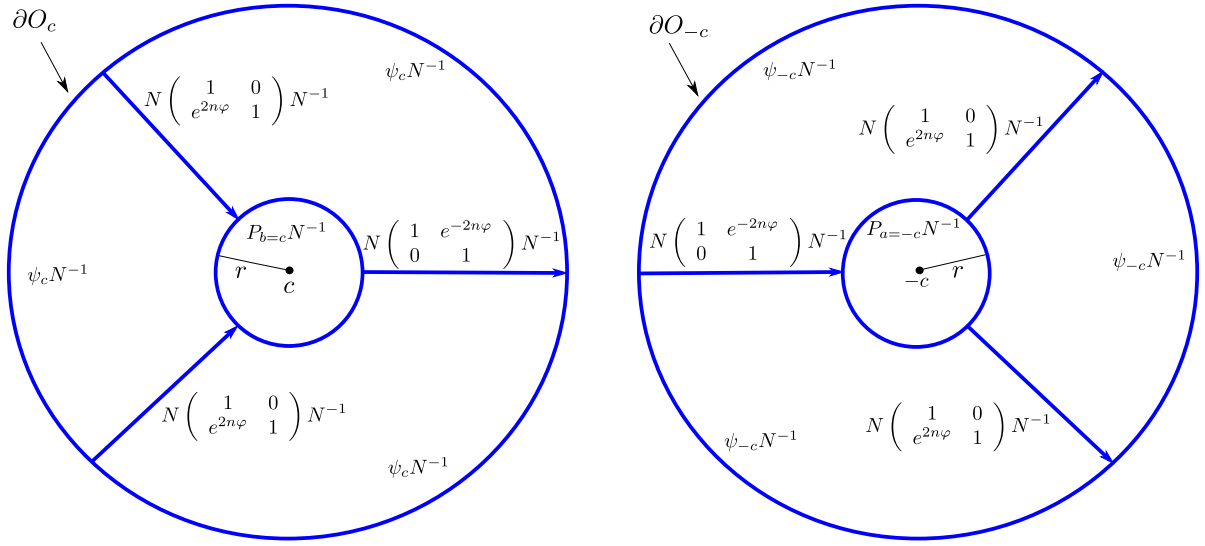

Figure 14: The separate RH problems for Ψ_c and Ψ_{-c}. The contours give a representation for Ω_n^c and Ω_n^{-c}. All circles have counter-clockwise orientation with $r \sim n^{-2/3}$. (a) The jump contours and jump matrices for Φ_c. (b) The jump contours and jump matrices for Φ_{-c}.

Lemma 5 *There exists a constant $C > 0$ and functions A_1, B_1 such that*

$$\begin{aligned} &G_1 J_c^{-1} = I + N[A_1(n^{-1}) + B_1(\epsilon)]N^{-1} \quad \textit{for} \quad |z-c| > r, \\ &G_1 J_c^{-1} = I, \quad \textit{for} \quad |z-c| = r \quad \textit{and}, \\ &\|\mathcal{C}[\bar{H}_1;\Omega_0]^{-1}\|_{\mathcal{L}(L^2(\Omega_0))} < C, \end{aligned} \tag{19}$$

where $\|A_1(n)\|_{L^2 \cap L^\infty} = \mathcal{O}(n)$ and $\|B_1(\epsilon)\|_{L^2 \cap L^\infty} = \mathcal{O}(\epsilon)$.

Proof For (19) it follows from scaling and truncation that for sufficiently large n, $G_1 - I$ is supported inside O_c. Furthermore, on $\Omega_c^n \setminus \partial O_c$, $J_c = G$ by construction so that (17) implies

$$N^{-1}G_\epsilon G^{-1}N = I + B_1(\epsilon),$$
$$G_\epsilon J_c^{-1} = I + NB_1(\epsilon)N^{-1}.$$

The analysis in in [8, p. 227] implies on ∂O_c

$$J_c^{-1} = I + A_1(n^{-1}),$$

Since $G_1 = I$ on ∂O_c we obtain (19). To prove the remainder of the lemma use unscaled jumps

$$\hat{H}_1(z) = \bar{H}_1(n^{2/3}(z-c)),$$
$$\hat{J}_c(z) = \begin{cases} \bar{N}_{b=c,n} J_c(z) \bar{N}_{b=c,n}^{-1} & \text{if } |z-c| > r, \\ J_c(z)\bar{N}_{b=c,n}^{-1} & \text{if } |z-c| = r. \end{cases}$$

From (19) we have

$$\|\hat{H}_1 \hat{J}_c^{-1} - I\|_{L^2 \cap L^\infty(\Omega_n^c)} = \mathcal{O}(n^{-1}) + \mathcal{O}(\epsilon).$$

It follows that $\|\hat{J}_c\|_{L^\infty(\Omega_n^c)}$ is uniformly bounded in n so that

$$\|\hat{H}_1 - \hat{J}_c\|_{L^2 \cap L^\infty(\Omega_n^c)} = \mathcal{O}(n^{-1}) + \mathcal{O}(\epsilon).$$

This implies $\|\mathcal{C}[\hat{H}_1; \Omega_n^c] - \mathcal{C}[\hat{J}_c; \Omega_n^c]\|_{\mathcal{L}(L^2(\Omega_0))} = \mathcal{O}(n^{-1}) + \mathcal{O}(\epsilon)$ since $\|\mathcal{C}^-_{\Omega_n^c}\|_{\mathcal{L}(L^2(\Omega_n^c))}$ is uniformly bounded in n. Therefore it suffices to show that $\|\mathcal{C}[\hat{J}_c; \Omega_n^c]^{-1}\|_{\mathcal{L}(L^2(\Omega_n^c))}$ is uniformly bounded in n. This is clear since the inverse operator can be written in terms of

$$\hat{\Psi}_c(z) = \begin{cases} \bar{N}_{a=c,n} \Psi_c \bar{N}_{a=c,n}^{-1}(z) & \text{if } z > r, \\ \bar{N}_{a=c,n}\Psi_c & \text{if } z < r. \end{cases} \tag{20}$$

and $\mathcal{C}^-_{\Omega_n^c}$, both of which are uniformly bounded in n on Ω_n^c. It remains to rescale the contours. We use a simple affine scaling and this leaves the Cauchy operators invariant: it does not affect the norm. In other words:

$$\|\mathcal{C}[\bar{H}_1; \Omega_0]^{-1}\|_{\mathcal{L}(L^2(\Omega_0))} = C \Leftrightarrow \|\mathcal{C}[\hat{H}_1; c + n^{-2/3}\Omega_0]^{-1}\|_{\mathcal{L}(L^2(c+n^{-2/3}\Omega_0))} = C.$$

The final step is to notice that $\mathcal{C}[\hat{H}_1; \Omega_n^c]^{-1}$ is the identity operator on $\Omega_n^c \setminus n^{2/3}(\Omega_0 - c)$. □

We now bound the inverse operator on the second solved RH problem.

Lemma 6 *There exists a constant $C > 0$ and functions A_2, B_2 such that*

$$\begin{aligned} &\tilde{G}_2 J_{-c}^{-1} = I + N[A_2(n^{-1}) + B_2(\epsilon)]N^{-1}, \quad \textit{for} \quad |z+c| > r, \\ &\tilde{G}_2 J_{-c}^{-1} = I + [A_2(n^{-1}) + B_2(\epsilon)]N^{-1}, \quad \textit{for} \quad |z+c| = r, \quad \textit{and,} \\ &\|\mathcal{C}[\bar{H}_2; \Omega_0]^{-1}\|_{\mathcal{L}(L^2(\Omega_0))} < C, \end{aligned} \tag{21}$$

where $\|A_2(n)\|_{L^2 \cap L^\infty} = \mathcal{O}(n)$ and $\|B_2(\epsilon)\|_{L^2 \cap L^\infty} = \mathcal{O}(\epsilon)$.

Proof First, for Φ_1 we have the representation

$$\Phi_1(z) = I + \bar{N}^{-1}_{b=c,n}\left(\mathcal{C}_{\Omega^1_n}U(z)\right)\bar{N}_{b=c,n}, \quad U(z) = u(n^{2/3}(z-c)), \quad u = \mathcal{C}[\bar{H}_1;\Omega_0]^{-1}(\bar{H}_1 - I).$$

Lemma 5 implies that u has uniformly bounded L^2 norm on Ω_0 so that a change of variables shows $\|U\|_{L^2(\Omega^1_n)} = \mathcal{O}(n^{-1/3})$. In addition, $\|1/(\cdot - z)^k\|_{L^2(\Omega^1_n)} = \mathcal{O}(n^{-1/3})$ for z bounded away from Ω^1_n. Therefore $|\mathcal{C}_{\Omega^1_n}U(z)| = \mathcal{O}(n^{-2/3})$. This estimate can be improved. Define

$$\tilde{U} = \mathcal{C}[J_c, \Omega^c_n]^{-1}(J_c - I).$$

It can be shown that $\|U - \tilde{U}\|_{L^2(\Omega^c_n)} = \mathcal{O}(\epsilon)\cdot\mathcal{O}(n^{-1/3}) + \mathcal{O}(n^{-4/3})$ where we use the convention that $U = 0$ on $\Omega^c_n \setminus \Omega^1_n$. Furthermore, $\mathcal{C}_{\Omega^c_n}\tilde{U} = 0$ on the compliment of $\overline{O}_c$ so that

$$\mathcal{C}_{\Omega^1_n}U = \mathcal{C}_{\Omega^1_n}U - \mathcal{C}_{\Omega^c_n}\tilde{U} \quad \text{on } \Omega^{-c}_n.$$

We find that $\|\mathcal{C}_{\Omega^1_n}U\|_{L^2\cap L^\infty(\Omega^{-c}_n)} = \mathcal{O}(\epsilon)\cdot\mathcal{O}(n^{-2/3}) + \mathcal{O}(n^{-5/3})$. We write

$$\Phi_1 = I + N(z)N^{-1}(z)\bar{N}^{-1}_{b=c,n}\left(\mathcal{C}_{\Omega^1_n}U(z)\right)\bar{N}_{b=c,n}N^{-1}(z),$$

and using that $N^{-1}(z)\bar{N}^{-1}_{b=c,n} = \mathcal{O}(n^{1/3})$ for $z \in \Omega^{-c}_n$ we find

$$\begin{aligned}\Phi_1 &= I + N[A_3(n^{-1}) + B_3(\epsilon)]N^{-1},\\ \Phi_1^{-1} &= I + N[A_4(n^{-1}) + B_4(\epsilon)]N^{-1}.\end{aligned}$$

where A_3, A_4 satisfy the property stated above for A_2 and B_3, B_4 satisfy the property stated for B_2. Expand

$$\begin{aligned}\tilde{G}_2J^{-1}_{-c} = G_2J^{-1}_{-c} &+ G_2N[A_3(n) + B_3(\epsilon)]N^{-1}J^{-1}_{-c}\\ &+ N[A_2(n^{-1}) + B_2(\epsilon)]N^{-1}G_2J^{-1}_{-c}\\ &+ N[A_2(n^{-1}) + B_2(\epsilon)]N^{-1}G_2N[A_3(n) + B_3(\epsilon)]N^{-1}J^{-1}_{-c}.\end{aligned}$$

We note that $N^{-1}G_2N$ and $N^{-1}J^{-1}_{-c}N$ are uniformly bounded on Ω^n_{-c} and $G_2J^{-1}_{-c}$ satisfies an analogous estimate as $G_1J^{-1}_c$ does in Lemma 5. So, we write

$$\begin{aligned}\tilde{G}_2J^{-1}_{-c} = I &+ N[A_1(n^{-1}) + B_1(\epsilon)]N^{-1}\\ &+ NN^{-1}G_2N[A_3(n^{-1}) + B_3(\epsilon)]N^{-1}J^{-1}_{-c}NN^{-1}\\ &+ N[A_2(n^{-1}) + B_2(\epsilon)]N^{-1}G_2J^{-1}_{-c}NN^{-1}\\ &+ N[A_2(n^{-1}) + B_2(\epsilon)]N^{-1}G_2N[A_3(n^{-1}) + B_3(\epsilon)]N^{-1}J^{-1}_{-c}NN^{-1}.\end{aligned}$$

This proves (21). The proof of the second statement proceeds in precisely the same way as in Lemma 5. This proves the lemma.

□

We can now bound the jump matrices.

Lemma 7 *There exists constants $C_k > 0$, independent of n, such that for sufficiently large n we have*

$$\|\bar{H}_i\|_{W^{k,\infty}\cap H^k(\Omega_0)} < C_k, \quad i = 1, 2.$$

Proof We consider $i = 1$ first. The only terms that may cause growth in the derivatives are

$$\kappa(z) = e^{-2n\varphi(c+n^{-2/3}z)} \quad \text{and} \quad N(c+n^{-2/3}z)\bar{N}_{b=c,n}.$$

From the analysis of [8, p. 197] it follows that $\varphi(z) = d_0(z-c)^{3/2}+d_1(z-c)^{5/2}+\mathcal{O}\left((z-c)^{7/2}\right)$. (This asymptotic series can be differentiated as $\sqrt{z-c}\varphi(z)$ is analytic.) Therefore,

$$\kappa(z) = \exp\left(-2d_0z^{3/2} - 2d_0n^{-2/3}z^{5/3} + \cdots\right).$$

and hence differentiating $\kappa(z)$ or $1/\kappa(z)$ with respect to z will never cause growth in n. Similar arguments apply to $N(c+n^{-2/3}z)\bar{N}_{b=c,n}$. From the expansion of $N(c+n^{-2/3}z)$ we have a series of the form

$$N(c+n^{-2/3}z)\bar{N}_{b=c,n} = f_0(z) + \sum_{j=1}^{\infty} M_{-(2j-1)/3}(n)f_j(z),$$

where $M_{-(2j+1)/3}(n) = \mathcal{O}(n^{-(2j+1)/3})$. Again, differentiation of $N(c+n^{-2/3}z)$ in z will never cause growth in n. This proves the claim for $i = 1$. For $i = 2$, we must bound derivatives of $\Phi_1(-c+n^{-2/3}z)$ and $\tilde{H}_2(z)$. The boundedness of the derivatives of $\tilde{H}_2(z)$ follows from the arguments for $i = 1$. Recall, for Φ_1 we have the representation

$$\Phi_1(z) = I + \bar{N}^{-1}_{b=c,n}\left(\mathcal{C}_{\Omega_n^1}U(z)\right)\bar{N}_{b=c,n}, \quad U(z) = u(n^{2/3}(z-c)), \quad u(z) = \mathcal{C}[\bar{H}_1;\Omega_0]^{-1}(\bar{H}_1 - I).$$

Since u has uniformly bounded L^2 norm on Ω_0, $\|U\|_{L^2(\Omega_n^1)} = \mathcal{O}(n^{-1/3})$. From the fact that $\bar{N}_{b=c,n},\ N^{-1}_{b=c,n} = \mathcal{O}(n^{1/6})$ we have that $\partial_z^k(\bar{N}^{-1}_{b=c,n}\left(\mathcal{C}_{\Omega_n^1}U(z)\right)\bar{N}_{b=c,n}) = \mathcal{O}(n^{-1/3})$ on Ω_n^2 where we used the fact that $\|1/(\cdot - z)^k\|_{L^2(\Omega_n^1)} = \mathcal{O}(n^{-1/3})$ for z bounded away from Ω_n^1. This proves the lemma for $i = 2$. □

In practice, we approximate Φ_1 so we never solve the exact RH problem $[\bar{H}_2;\Omega_0]$. Recall this approximation is found by first numerically approximating the solution $\bar{\Phi}_1$ of $[\bar{H}_1;\Omega_0]$ by $\bar{\Phi}_{1,m}$ (with m collocation points on each smooth component of Ω_0). Theorem 2 shows that the approximation $\bar{\Phi}_{1,m}$ will converge uniformly in n and z away from Ω_0 as $m \to \infty$ (subject to Assumption 1). The size of the difference $\bar{\Phi}_{1,m} - \bar{\Phi}_1$ can be traced back to an L^2 error on Ω_0. In other words,

$$\bar{\Phi}_{1,m}(z) = I + \mathcal{C}_{\Omega_0}u_m(z) \quad \text{and} \quad \bar{\Phi}_1(z) = I + \mathcal{C}_{\Omega_0}u(z),$$

where $\|u - u_m\|_{L^2(\Omega_0)} \to 0$ is satisfied as $m \to \infty$. It follows from Cauchy–Schwarz that

$$|\bar{\Phi}_{1,m}(n^{2/3}(z-c)) - \bar{\Phi}_1(n^{2/3}(z-c))| < \|1/(\cdot - n^{2/3}(z-c))\|_{L^2(\Omega_0)}\|u - u_m\|_{L^2(\Omega_0)}n^{-2/3}.$$

Therefore from $\bar{N}_{b=c,n},\ N^{-1}_{b=c,n} = \mathcal{O}(n^{1/6})$, we bound

$$\|\Phi_{1,m} - \Phi_1\|_{L^\infty(\Omega_n^2)} \le C\|u - u_m\|_{L^2(\Omega_0)}n^{-1/3}.$$

Similar arguments show

$$\|\Phi_{1,m}^{-1} - \Phi_1^{-1}\|_{L^\infty(\Omega_n^2)} \le C\|u - u_m\|_{L^2(\Omega_0)}n^{-1/3} + \mathcal{O}(n^{-2/3}).$$

Define $\bar{H}_{2,m}$ to be $\bar{H}_2$ with Φ_1 replaced by $\Phi_{1,m}$. The final lemma we need for our fundamental result of this section follows.

Lemma 8

$$\|\bar{H}_{2,m} - \bar{H}_2\|_{L^2\cap L^\infty(\Omega_0)} \to 0 \text{ as } m \to \infty,$$

uniformly in n.

Proof The case $|z+c| > r$ is treated first. We use the unscaled jump matrices to show L^∞ convergence. consider

$$\begin{aligned}\bar{H}_{2,m}(n^{2/3}(z+c)) - \bar{H}_2(n^{2/3}(z+c)) \\ &= \bar{N}_{a=-c,n}\Phi_1(z)G_2(z)\Phi_1^{-1}(z)\bar{N}^{-1}_{a=-c,n} - \bar{N}_{a=-c,n}\Phi_{1,m}(z)G_2(z)\Phi^{-1}_{1,m}(z)\bar{N}^{-1}_{a=-c,n} \\ &= \bar{N}_{a=-c,n}(\Phi_1(z) - \Phi_{1,m}(z))\bar{N}^{-1}_{a=-c,n}\bar{N}_{a=-c,n}G_2(z)\bar{N}^{-1}_{a=-c,n}\bar{N}_{a=-c,n}\Phi_1^{-1}(z)\bar{N}^{-1}_{a=-c,n} \\ &+ \bar{N}_{a=-c,n}\Phi_{1,m}(z)\bar{N}^{-1}_{a=-c,n}\bar{N}_{a=-c,n}G_2(z)\bar{N}^{-1}_{a=-c,n}\bar{N}_{a=-c,n}(\Phi_1^{-1}(z) - \Phi^{-1}_{1,m})\bar{N}^{-1}_{a=-c,n}\end{aligned}$$

We have seen that

$$\begin{aligned}\bar{N}_{a=-c,n}\Phi_{1,m}(z)\bar{N}^{-1}_{a=-c,n} &= \mathcal{O}(1), \\ \bar{N}_{a=-c,n}\Phi_1(z)\bar{N}^{-1}_{a=-c,n} &= \mathcal{O}(1), \\ N_{a=-c,n}G_2(z)\bar{N}^{-1}_{a=-c,n} &= \mathcal{O}(1),\end{aligned}$$

and finally

$$\begin{aligned}\|\bar{N}_{a=-c,n}(\Phi_1 - \Phi_{1,m})\bar{N}^{-1}_{a=-c,n}\|_{L^\infty(\Omega_n^2)} &\le C\|u-u_m\|_{L^2(\Omega_0)}, \\ \|\bar{N}_{a=-c,n}(\Phi_1^{-1} - \Phi^{-1}_{1,m})\bar{N}^{-1}_{a=-c,n}\|_{L^\infty(\Omega_n^2)} &\le C\|u-u_m\|_{L^2(\Omega_0)} + \mathcal{O}(n^{-1/3})\cdot\mathcal{O}(\|u-u_m\|^2_{L^2(\Omega_0)}).\end{aligned}$$

for a new constant C. This demonstrates that $\|\bar{H}_{2,m} - \bar{H}_2\|_{L^2\cap L^\infty(\Omega_0)} \to 0$ uniformly in n since Ω_0 is bounded. The case of $|z+c| < r$ follows form this analysis since fewer $\bar{N}_{a=-c,n}$ terms are present in that case. □

As before, let $u = \mathcal{C}[\bar{H}_1;\Omega_1]^{-1}(\bar{H}_1 - I)$ with u_m being its numerical approximation. Define $v = \mathcal{C}[\bar{H}_2;\Omega_2]^{-1}(\bar{H}_2 - I)$ and $v^m = \mathcal{C}[\bar{H}_{2,m};\Omega_2]^{-1}(\bar{H}_{2,m} - I)$. Let v_m denote the numerical approximation of v^m and define

$$\Phi_{2,m} = \bar{N}^{-1}_{a=-c,n}(I + \mathcal{C}_{\Omega_0}v_m(n^{2/3}(z+c))N_{a=-c,n},$$

which is an approximation of Φ_2.

We are now ready to prove our main extension of the uniform approximation theory.

Theorem 4 *The following limits hold, uniformly with respect to n:*

$$\begin{aligned}\|u-u_m\|_{L^2(\Omega_0)} \to 0 \quad as \quad m\to\infty, \\ \|v-v_m\|_{L^2(\Omega_0)} \to 0 \quad as \quad m\to\infty.\end{aligned}$$

Furthermore,

$$\lim_{m\to\infty}\sup_{z\in S}|\Phi(z) - \Phi_{1,m}(z)\Phi_{2,m}(z)| = \mathcal{O}(\epsilon)$$

for S bounded away from Γ_n where ϵ is the error associated with contour truncation, see (17)*.*

Proof The first limit was proved above. Lemma 8 implies $\|v^m - v\|_{L^2(\Omega_0)} \to 0$ uniformly in n. The triangle inequality produces the second limit. Finally, Cauchy–Schwarz applied the Cauchy integral implies

$$\lim_{m\to\infty}\sup_{z\in S}|\Phi(z) - \Phi_{1,m}(z)\Phi_{2,m}(z)| = 0,$$

uniformly in n. Combining this with (17) proves the theorem. □

6 Conclusion

We presented a numerical method for computing statistics of unitary invariant ensembles, based on solving the associated Riemann–Hilbert problem numerically. This required solving a scalar Riemann–Hilbert problem to calculate the g function associated with the equilibrium measure. Scaling the contours appropriately resulted in a numerical method that remains accurate for large n, without knowledge of the local parametrices. We showed that the accuracy of the resulting numerical method, under Assumption 1, was uniformly accurate in n.

Our hope is that this framework leads to a better understanding of the relationship between the potential V, universality laws and finite n statistics.

A Computing a Hastings–McLeod Solution of the Painlevé II transcendent

Here we focus on the (homogeneous) Painlevé II ODE, it is as follows:

$$u''(x) = xu(x) + 2u^3(x). \tag{22}$$

(For brevity we refer to the homogeneous Painlevé II simply as Painlevé II.) There are many important applications of this equation: as mentioned above, the Tracy–Widom distribution [33] is written in terms of the Hastings–McLeod solution q [20]:

$$\begin{aligned} \det(I - \mathcal{A}|_{L^2(s,\infty)}) &= \exp\left(-\int_s^\infty (x-s)q^2(x)\,\mathrm{d}x\right) \quad \text{for} \\ q''(x) &= xq(x) + 2q^3(x) \qquad \text{and} \qquad q(x) \sim -\mathrm{Ai}\,(x) \quad \text{as} \quad x \to \infty. \end{aligned}$$

Furthermore, it has also been shown that asymptotic solutions to the Korteweg–de Vries and modified Korteweg–de Vries equations can be written in terms of Ablowitz–Segur solutions [1]. The aim of this section is to demonstrate that the RH formulation can indeed be used effectively to compute solutions to Painlevé II, even in the asymptotic regime.

Solutions to differential equations such as (22) are typically defined by initial conditions: at a point x we are given $u(x)$ and $u'(x)$. In the RH formulation, however, we do not specify initial conditions. Rather, the solution is specified by the *Stokes' constants*; constants s_1, s_2, s_3 which satisfy the following condition:

$$s_1 - s_2 + s_3 + s_1 s_2 s_3 = 0. \tag{23}$$

We treat the Stokes' constants as given, as, in many applications they arise naturally whilst initial conditions do not. Given such constants, we denote the associated solution to (22) by

$$P_{\mathrm{II}}(s_1, s_2, s_3; z). \tag{24}$$

P_{II} and its derivative can be viewed as the special functions which map Stokes' constants to initial conditions.

At first glance, computing solutions to (22) appears trivial: given initial conditions, simply use one's favourite time-stepping algorithm, e.g., input it into an ODE toolbox such as MATLAB's `ode45` or MATHEMATICA's `NDSolve`. Unfortunately, several difficulties immediately become apparent. In Figure 15, we plot several solutions to (22) (computed using

the approach we are advocating): the Hastings–McLeod solution and perturbations of the Hastings–McLeod solution. Note that the solution is inherently unstable, and small perturbations cause oscillations — which make standard ODE solvers inefficient — and poles — which completely breaks such ODE initial value problem solvers (the issue of poles can be resolved using the methodology of [18]).

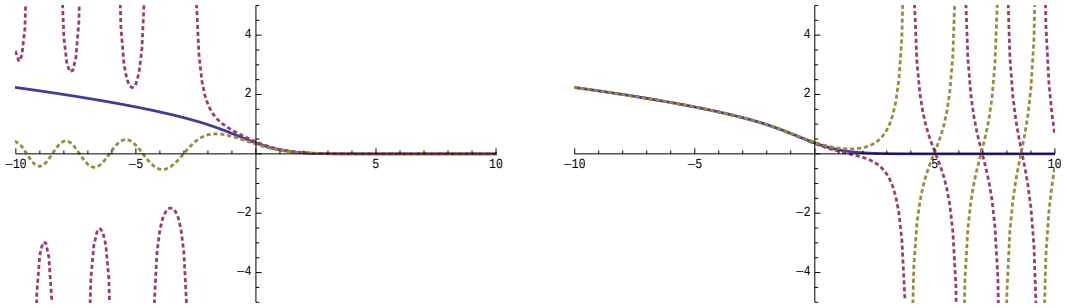

Figure 15: Solutions to Painlevé II, with the Hastings–McLeod solution in solid, showing that an initial value solver for Hastings–McLeod must be unstable. (a) Small perturbations at the right end integrated left. (b) Small perturbations at the left end integrated right.

Remark There are many other methods for computing the Tracy–Widom distribution itself as well as the Hastings–McLeod solution [5, 4], based on the Fredholm determinant formulation or solving a boundary value problem. Moreover, accurate data values have been tabulated using high precision arithmetic with a Taylor series method [29, 30]. However, we see that there is a whole family of solutions to Painlevé II which exhibit similar sensitivity to initial conditions, and thus a reliable, general numerical method is needed even for this case. We note that the approach [18], which combines boundary value problem solvers with initial value problem solvers, may also be successful for calculating such solutions. However, it only works with initial conditions, not with Stokes' constants.

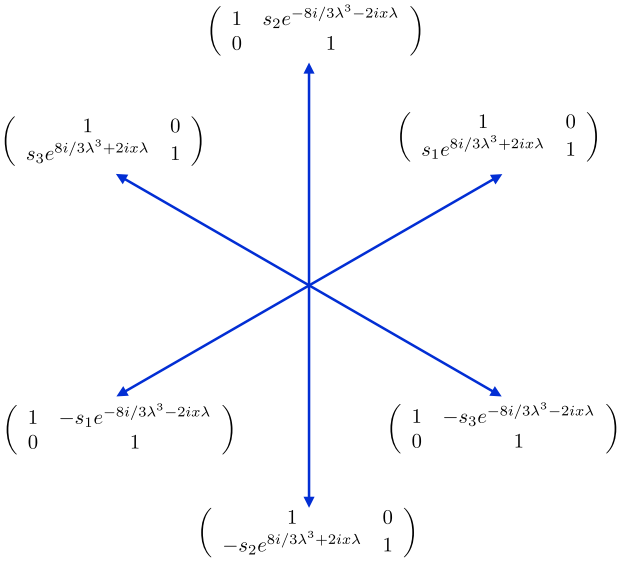

Figure 16: The contour and jump matrix for the Painlevé II RH problem.

Let $\Phi(x;\lambda)$ solve the RH problem depicted in Figure 16: let $\Gamma = \Gamma_1 \cup \cdots \cup \Gamma_6$ for $\Gamma_\kappa\{se^{i\pi(\kappa/3-1/6)} : s \in \mathbb{R}^+\}$, *i.e.*, Γ consists of six rays emanating from the origin, as see in

Figure 16. Then the jump matrix is defined by $G(x;\lambda) = G_\kappa(x;\lambda)$ for $z \in \Gamma_\kappa$, where

$$G_\kappa(x;\lambda) = G_\kappa(\lambda) = \begin{cases} \begin{pmatrix} 1 & s_\kappa e^{-i8/3\lambda^3 - 2ix\lambda} \\ 0 & 1 \end{pmatrix} & \text{if } \kappa \text{ even}, \\ \begin{pmatrix} 1 & 0 \\ s_\kappa e^{i8/3\lambda^3 + 2ix\lambda} & 1 \end{pmatrix} & \text{if } \kappa \text{ odd}, \end{cases}$$

with $s_4 = -s_1$,$s_5 = -s_2$ and $s_6 = -s_3$. This is the RH problem which was solved numerically in [26]. We recover the corresponding solution to Painlevé II from Φ by [16]

$$P_{\mathrm{II}}(s_1, s_2, s_3; x) = 2\mathrm{i} \lim_{\lambda\to\infty} \lambda\Phi(x;\lambda)_{12}.$$

As $|x|$ becomes large, the jump matrices G are increasingly oscillatory. We combat this issue by deforming the contour so that these oscillations become exponential decay. To simplify this procedure, we first rescale the RH problem. Note that, if we let $z = \sqrt{|x|}\lambda$, then the jump contour Γ remains unchanged, and

$$\tilde{\Phi}^+(z) = \Phi^+(x; z/\sqrt{|x|}) = \Phi^-(x; z/\sqrt{|x|})G(z/\sqrt{|x|}) = \tilde{\Phi}^-(z)\tilde{G}(z),$$

where $\tilde{G}(z) = G_\kappa(z/\sqrt{|x|})$ on Γ_κ for

$$G_\kappa(z/\sqrt{|x|}) = \begin{cases} \begin{pmatrix} 1 & s_\kappa e^{-i|x|^{3/2}\theta(z)} \\ 0 & 1 \end{pmatrix} & \text{if } \kappa \text{ even}, \\ \begin{pmatrix} 1 & 0 \\ s_\kappa e^{i|x|^{3/2}\theta(z)} & 1 \end{pmatrix} & \text{if } \kappa \text{ odd}, \end{cases}$$

and

$$\theta(z) = \frac{2}{3}\left(4z^3 + 2e^{i\arg x} z\right).$$

Then

$$P_{\mathrm{II}}(s_1, s_2, s_3; x) = 2i \lim_{\lambda\to\infty} \lambda\Phi(x;\lambda)_{12} = 2i\sqrt{|x|} \lim_{z\to\infty} z\tilde{\Phi}(z)_{12}.$$

A.1 Positive x with $s_2 = 0$

We deform the RH problem for Painlevé II so that numerics are asymptotically stable for positive x. The deformation is extremely simple under the following special case:

$$s_2 = 0 \tag{25}$$

We remark that, unlike other deformations, the following deformation can be easily extended to achieve asymptotic stability for x in the complex plane such that $-\frac{\pi}{3} < \arg x < \frac{\pi}{6}$.

On the undeformed contour, the terms $e^{\pm i|x|^{3/2}\theta(z)}$ become oscillatory as $|x|$ becomes large. However, with the right choice of curve $h(t)$, $e^{\pm i\theta(h(t))}$ has no oscillations; instead, it decays exponentially fast as $t \to \infty$. But h is precisely the path of steepest descent, which passes through the stationary points of θ, *i.e.*, the points where the derivative of θ vanishes. We readily find that

$$\theta'(z) = 2(4z^2 + 1),$$

and the stationary points are $z = \pm i/2$.

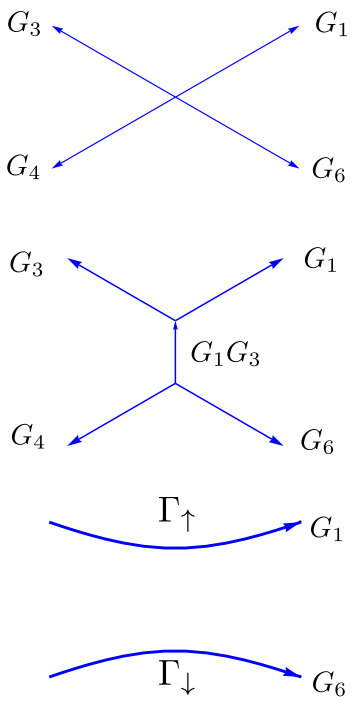

Figure 17: Deforming the RH problem for positive x, assuming (25).

We note that, since $G_2 = I$, when we deform Γ_1 and Γ_3 through $i/2$ they become completely disjoint from Γ_4 and Γ_6, which we then deform through $-i/2$. We also point out that $G_3^{-1} = G_1$ and $G_6^{-1} = G_4$; thus we reverse the orientation of Γ_3 and Γ_4. Define $\Gamma_\uparrow$ to be the curve G_1 is defined on and $\Gamma_\downarrow$ be the contour G_4 is defined on, as seen in Figure 17.

Now recall that

$$\theta\left(\pm\frac{i}{2}\right) = \pm\frac{i}{3}.$$

However, we only have $\Gamma_\uparrow$ emanating from $i/2$, with jump matrix

$$G_1 = \begin{pmatrix} 1 & 0 \\ s_1 e^{i|x|^{3/2}\theta(z)} & 1 \end{pmatrix}.$$

This is exponentially decaying to the identity along $\Gamma_\uparrow$; as is G_4 along $\Gamma_\downarrow$. We employ the approach of Section 3.2. We first use Lemma 3 to truncate the contours near the stationary point. What remains is to determine what near means. Because θ behaves like $\mathcal{O}\left(z \pm i/2\right)^2$ near the stationary points, Assumption 2 implies that we should choose the shifting of $\beta_1 = i/2$ and $\beta_2 = -i/2$, the scalings $\alpha_1 = \alpha_2 = r|x|^{-3/4}$ and the canonical domains $\Omega_1 = \Omega_2 = [-1, 1]$. Here r is chosen so that what is truncated is negligible in the sense of Lemma 3. G_6 is similar. The complete proof of asymptotic stability follows from Theorem 2.

A.2 Negative x with $s_1 = -s_3 = \pm i$ and $s_2 = 0$

We now develop deformations for the Hastings–McLeod solution for negative x, which corresponds to $s_1 = \pm\mathrm{i}$, $s_2 = 0$ and $s_3 = \mp\mathrm{i}$ [16]. We realize numerical asymptotic stability in the aforementioned sense for the following special case:

$$s_1 = -s_3 = \pm i \qquad \text{and} \qquad s_2 = 0 \tag{26}$$

We begin by deforming the RH problem (Figure 16) to the one shown in Figure 18. The horizontal contour extends from $-\alpha$ to α for $\alpha > 0$. We determine α below. Define

$$G_0 = G_6 G_1 = \begin{pmatrix} 0 & s_1 e^{-i|x|^{3/2}\theta(z)} \\ s_1 e^{i|x|^{3/2}\theta(z)} & 1 \end{pmatrix}.$$

Note that the assumption $s_2 = 0$ simplifies the form of the RH problem substantially, see Figure 18(b). We use an approach similar to that of the equilibrium measure to replace θ

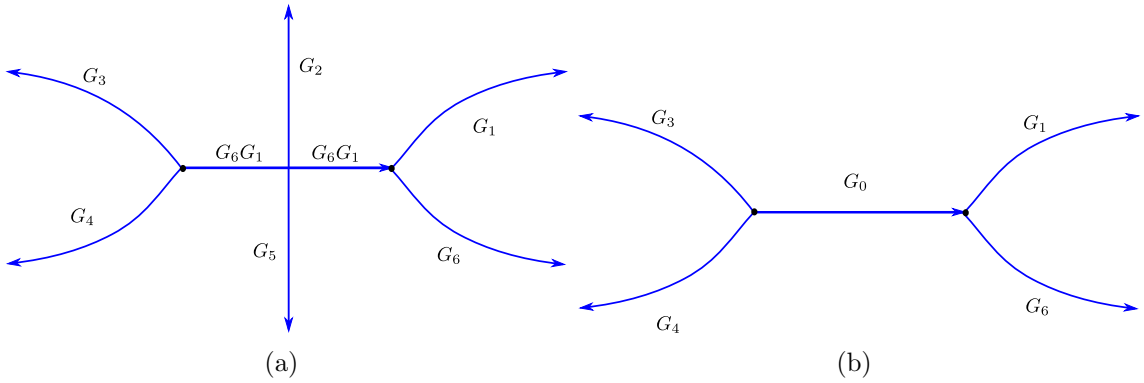

Figure 18: Deforming the RH problem for negative x, assuming (26). The black dots represent $\pm\alpha$. (a) Initial deformation for $s_2 \neq 0$. (b) Simplification following from $s_2 = 0$.

with a function possessing more desirable properties. Define

$$\Theta(z) = e^{i|x|^{3/2}\frac{g(z)-\theta(z)}{2}\sigma_3}, \quad \sigma_3 = \begin{pmatrix} 1 & 0 \\ 0 & -1 \end{pmatrix}, \quad g(z) = (z^2 - \alpha^2)^{3/2}.$$

The branch cut for $g(z)$ is chosen along $[-\alpha, \alpha]$. If we set $\alpha = 1/\sqrt{2}$ the branch of g is chosen so that $g(z) - \theta(z) \sim \mathcal{O}(z^{-1})$. Furthermore, $g_+(z) + g_-(z) = 0$ and $\mathrm{Im}(g_-(z) - g_+(z)) > 0$ on $(-\alpha, \alpha)$. Define $\hat{G}_i = \Theta_-^{-1} G_i \Theta_+$ and note that

$$\hat{G}_0(z) = \begin{pmatrix} 0 & s_1 e^{-i|x|^{3/2}\frac{g_+(z)+g_-(z)}{2}} \\ s_1 e^{i|x|^{3/2}\frac{g_+(z)+g_-(z)}{2}} & e^{i|x|^{3/2}\frac{g_-(z)-g_-(z)}{2}} \end{pmatrix} = \begin{pmatrix} 0 & s_1 \\ s_1 & e^{i|x|^{3/2}\frac{g_-(z)-g_-(z)}{2}} \end{pmatrix}.$$

As $x \to -\infty$, G_0 tends to the matrix

$$J = \begin{pmatrix} 0 & s_1 \\ s_1 & 0 \end{pmatrix}.$$

The solution of the RH problem

$$\Psi^+(z) = \Psi^-(z) J, \quad z \in [-\alpha, \alpha], \quad \Psi(\infty) = I,$$

is given by

$$\Psi_{\mathrm{HM}}^{\mathrm{out}}(z) = \frac{1}{2} \begin{pmatrix} \beta(z) + \beta(z)^{-1} & -is_1(\beta(z) - \beta(z)^{-1}) \\ -is_1(\beta(z) - \beta(z)^{-1}) & \beta(z) + \beta(z)^{-1} \end{pmatrix}, \quad \beta(z) = \left(\frac{z-\alpha}{z+\alpha}\right)^{1/4}.$$

Here β has a branch cut on $[-\alpha, \alpha]$ and satisfies $\beta(z) \to 1$ as $z \to \infty$. It is clear that $(\Psi_{\mathrm{HM}}^{\mathrm{out}})_+ \hat{G}_0 (\Psi_{\mathrm{HM}}^{\mathrm{out}})_-^{-1} \to I$ uniformly on every closed subinterval of $(-\alpha, \alpha)$.

We define local parametrices near $\pm\alpha$:

$$\Psi_{\rm HM}^{\alpha} = \begin{cases} I & \text{if } -\frac{\pi}{3} < \arg(z-\alpha) < \frac{\pi}{3} \\ \hat{G}_1^{-1} & \text{if } \frac{\pi}{3} < \arg(z-\alpha) < \pi \\ \hat{G}_1 & \text{if } -\pi < \arg(z-\alpha) < -\frac{\pi}{3} \end{cases},$$

$$\Psi_{\rm HM}^{-\alpha} = \begin{cases} I & \text{if } \frac{2\pi}{3} < \arg(z+\alpha) < \pi \text{ or } -\pi < \arg(z+\alpha) < -\frac{2\pi}{3} \\ \hat{G}_1^{-1} & \text{if } 0 < \arg(z+\alpha) < \frac{2\pi}{3} \\ \hat{G}_1 & \text{if } -\frac{2\pi}{3} < \arg(z+\alpha) < \frac{2\pi}{3} \end{cases}.$$

We are ready to define the global parametrix. Given $r > 0$ define

$$\Psi_{\rm HM} = \begin{cases} \Psi_{\rm HM}^{\alpha} & \text{if } |z-\alpha| < r \\ \Psi_{\rm HM}^{-\alpha} & \text{if } |z+\alpha| < r \\ \Psi_{\rm HM}^{\rm out} & \text{if } |z+\alpha| > r \text{ and } |z-\alpha| > r \end{cases}.$$

It follows that $\Psi_{\rm HM}$ satisfies the RH problem shown in Figure A.2.

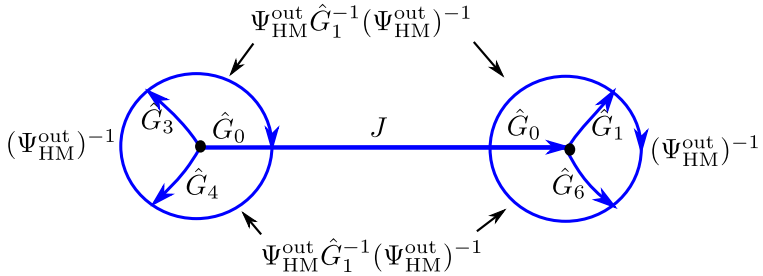

Figure 19: The jump contours and jump matrices for the RH problem solved by $\Psi_{\rm HM}$. The radius for the two circles is r.

Let $\hat{\Phi}$ be the solution of the RH problem shown in Figure 20(a). It follows that $\Delta = \hat{\Phi}\Psi_{\rm HM}^{-1}$ solves the RH problem shown in Figure 20(b). The RH problem for Δ has jump matrices

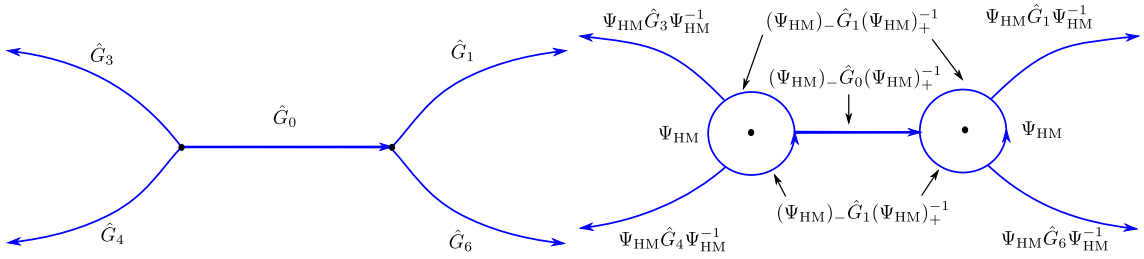

Figure 20: The final deformation of the RH problem for negative x, assuming (26). The black dots represent $\pm\alpha$. (a) After conjugation by Θ. (b) Bounding the contours away from the singularities of g and β using $\Psi_{\rm HM}$.

that decay to the identity away from $\pm\alpha$. We use Assumption 2 to determine that we should use $r = |x|^{-1}$. We solve the RH problem for Δ numerically. To compute the solution of Painlevé II we use the formula

$$P_{\rm II}(\pm \mathrm{i}, 0, \mp \mathrm{i}; x) = 2i\sqrt{|x|} \lim_{z\to\infty} z\Delta(z)_{12}.$$

See Figure 15 for a plot of the Hastings–McLeod solution with $s_1 = -i$. To verify our computations we may we use the asymptotics [16]:

$$P_{\mathrm{II}}(-i, 0, i; x) \sim \sqrt{\frac{-x}{2}} + \mathcal{O}\left(x^{-5/2}\right). \tag{27}$$

We use

$$D_{\mathrm{HM}}(x) = \left| \frac{P_{\mathrm{II}}(-\mathrm{i}, 0, \mathrm{i}; x)}{\sqrt{\frac{-x}{2}}} - 1 \right|,$$

as an indicator of of the relative error, which should tend to zero for x large and negative. We demonstrate this in Figure 21(a).

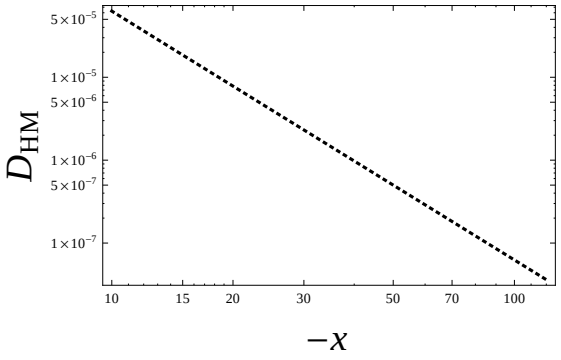

(a)

Figure 21: Analysis of the numerical approximation of $P_{\mathrm{II}}(-\mathrm{i}, 0, \mathrm{i}; x)$. (See Figure 15 for a plot of the solution for positive and negative x. For small $|x|$ we solve the undeformed RH problem.) A verification the numerical approximation using the asymptotics (27).

Remark Since β has unbounded singularities we expect that a similar issue as in Section 5.2.2 will arise. We do not go though the details of this but this approach produces accurate numerics for all x on the real line.

References

[1] M. J. Ablowitz and H. Segur. Asymptotic solutions of the Korteweg–de Vries equation. *Stud. in Appl. Math.*, 57:13–44, 1977.

[2] Gernot Akemann, Jinho Baik, and Philippe Di Francesco. *The Oxford handbook of random matrix theory*. Oxford University Press, 2011.

[3] G Anderson, Alice Guionnet, and Ofer Zeitouni. *Introduction to random matrices (Studies in advanced mathematics, N 118)*. Cambridge University Press, Cambridge, 2009.

[4] F. Bornemann. On the numerical evaluation of distributions in random matrix theory. *Markov Process. Related Fields*, 2010.

[5] F. Bornemann. On the numerical evaluation of Fredholm determinants. *Maths. Comp.*, 79:871–915, 2010.

[6] T. Claeys, I. Krasovsky, and A. Its. Higher-order analogues of the Tracy–Widom distribution and the Painlevé II hierarchy. *Comm. Pure Appl. Math.*, 63:362–412, 2010.

[7] T. Claeys and S. Olver. Numerical study of higher order analogues of the Tracy–Widom distribution. *Cont. Maths*, 578:83–99, 2011.

[8] P. Deift. *Orthogonal Polynomials and Random Matrices: a Riemann–Hilbert Approach.* AMS, 2000.

[9] P. Deift and D. Gioev. Universality at the edge of the spectrum for unitary, orthogonal, and symplectic ensembles of random matrices. *Comm. Pure Appl. Math.*, 60(6):867–910, 2007.

[10] P. Deift, T. Kriecherbauer, and K. T.-R. McLaughlin. New results on the equilibrium measure for logarithmic potentials in the presence of an external field. *J. Approx. Theory*, 95(3):388–475, 1998.

[11] P. Deift, T. Kriecherbauer, K. T-R McLaughlin, S. Venakides, and X. Zhou. Asymptotics for polynomials orthogonal with respect to varying exponential weights. *Internat. Math. Res. Notices*, 1997(16):759–782, 1997.

[12] P. Deift, T. Kriecherbauer, K. T-R McLaughlin, S. Venakides, and X. Zhou. Strong asymptotics of orthogonal polynomials with respect to exponential weights. *Comm. Pure Appl. Math.*, 52(12):1491–1552, 1999.

[13] P. Deift, T. Kriecherbauer, K. T.-R. McLaughlin, S. Venakides, and X. Zhou. Uniform asymptotics for polynomials orthogonal with respect to varying exponential weights and applications to universality questions in random matrix theory. *Comm. Pure Appl. Math.*, 52(11):1335–1425, 1999.

[14] Percy Deift and Dimitri Gioev. *Random matrix theory: invariant ensembles and universality*, volume 18. Amer Mathematical Society, 2009.

[15] Alan Edelman and N Raj Rao. Random matrix theory. *Acta Numerica*, 14(1):233–297, 2005.

[16] A. S. Fokas, A. R. Its, A. A. Kapaev, and V. Y. Novokshenov. *Painlevé Transcendents: the Riemann–Hilbert Approach.* AMS, 2006.

[17] A. S. Fokas, A. R. Its, and A. V. Kitaev. The isomonodromy approach to matric models in 2d quantum gravity. *Comm. Math. Phys.*, 147(2):395–430, 1992.

[18] B. Fornberg and J. A. C. Weideman. A numerical methodology for the Painlevé equations. *J. Comp. Phys.*, 2011.

[19] W. Gautschi. *Orthogonal Polynomials: Applications and Computation.* Oxford University Press, 2004.

[20] S. P. Hastings and J. B. McLeod. A boundary value problem associated with the second Painlevé transcendent and the Korteweg–de Vries equation. *Arc. Rat. Mech. Anal.*, 73:31–51, 1980.

[21] M.L. Mehta. *Random Matrices.* Academic Press, 2004.

[22] HN Mhaskar and EB Saff. Extremal problems for polynomials with exponential weights. *Trans. Amer. Math. Soc*, 285(1):203–234, 1984.

[23] F. W. J. Olver, D. W. Lozier, R. F. Boisvert, and C. W. Clark. *NIST Handbook of Mathematical Functions*. Cambridge University Press, 2010.

[24] S. Olver. Computation of equilibrium measures. *J. Approx. Theory*, 163:1185–1207, 2011.

[25] S. Olver. Computing the Hilbert transform and its inverse. *Math. Comp.*, 80:1745–1767, 2011.

[26] S. Olver. Numerical solution of Riemann–Hilbert problems: Painlevé II. *Found. Comput. Math.*, 11:153–179, 2011.

[27] S. Olver. A general framework for solving Riemann–Hilbert problems numerically. *Numer. Math.*, 122:305–340, 2012.

[28] S. Olver and T. Trogdon. Nonlinear steepest descent and the numerical solution of Riemann–Hilbert problems. `arXiv:1205.5604 [math.NA]`, 2012.

[29] M. Prähofer and H. Spohn. Exact scaling functions for one-dimensional stationary KPZ growth. http://www-m5.ma.tum.de/KPZ/.

[30] M. Prähofer and H. Spohn. Exact scaling functions for one-dimensional stationary KPZ growth. *J. Stat. Phys.*, 115:255–279, 2004.

[31] Evguenii Andreevich Rakhmanov. On asymptotic properties of polynomials orthogonal on the real axis. *Matematicheskii Sbornik*, 161(2):163–203, 1982.

[32] E. B. Saff and V. Totik. *Logarithmic Potentials with External Fields*. Springer, 1997.

[33] C. A. Tracy and H. Widom. Level-spacing distributions and the Airy kernel. *Comm. Math. Phys.*, 159:151–174, 1994.

[34] G. Wechslberger and F. Bornemann. Automatic deformation of Riemann–Hilbert problems with applications to the Painlevé II transcendents. `arXiv:1206.2446 [math.NA]`, 2012.